

A simple stochastic quadrant model for the transport and deposition of particles in turbulent boundary layers

C. Jin,¹ I. Potts,¹ and M. W. Reeks^{1, a)}

*School of Mechanical & Systems Engineering, Newcastle University,
Stephenson Building, Claremont Road, Newcastle upon Tyne, NE1 7RU,
UK*

(Dated: 3 June 2014)

We present a simple stochastic quadrant model for calculating the transport and deposition of heavy particles in a fully developed turbulent boundary layer based on the statistics of wall-normal fluid velocity fluctuations obtained from a fully developed channel flow. Individual particles are tracked through the boundary layer via their interactions with a succession of random eddies found in each of the quadrants of the fluid Reynolds shear stress domain in a homogeneous Markov chain process. Deposition rates for a range of heavy particles predicted by the model compare well with benchmark experimental measurements. In addition deposition rates are compared with those obtained from continuous random walk (CRW) models including those based on a Langevin equation for the turbulent fluctuations. Various statistics related to the particle near wall behavior are also presented.

Keywords: Turbulent deposition, quadrant analysis, stochastic model, heavy particles, boundary layer

^{a)}Electronic mail: mike.reeks@ncl.ac.uk

I. INTRODUCTION

In this paper, we propose a simple stochastic quadrant model of coherent structures for heavy particle deposition in a turbulent boundary layer inspired by the quadrant analysis of Willmarth and Lu¹ which captures the influence of sweeps and ejections on the deposition of particles. It is another way of modeling deposition of heavy particles within fully developed turbulent boundary layers that adds insight and suggests new ways for improving the deposition prediction of heavy particles encountered in a wide range of industrial and environmental applications².

The modelling and simulation of the transport and deposition of particles in a turbulent boundary layer is a much studied topic. The first attempts of Friedlander and Johnstone³ and Davies⁴ were based on a gradient diffusion/free-flight theory where the concept of a particle stop distance was proposed. However the initial particle free-flight velocity had to be artificially adjusted from its value based on the local fluid rms velocity to get good agreement with the experimental data. Hutchinson *et al.*⁵ and Kallio and Reeks⁶ employed a Monte-Carlo based Lagrangian particle tracking method for calculating particle deposition. In the work of Kallio and Reeks⁶ the turbulent boundary layer was described as a randomized eddy field with corresponding velocity and time scales as functions of the particle distance away from the wall. Swailes and Reeks⁷ proposed to use the kinetic equation developed by Reeks⁸ as a model to study the deposition of “high inertia” particles in a turbulent duct flow. Young and Leeming⁹ developed a simple approach based on an advection diffusion equation (ADE) to address the particle deposition in turbulent pipe flows, which represents a considerable advance in physical understanding over previous free-flight theories. Guha¹⁰ developed a unified Eulerian theory, which is based on a Reynolds averaging of the particle continuity and momentum conservation equations for studying turbulent deposition onto smooth and rough surfaces. Zaichik *et al.*¹¹ developed a simplified Eulerian model called the diffusion-inertia model (DIM), which is based on a kinetic equation for the probability density function (PDF) of particle velocity and position, to investigate the dispersion and deposition of low-inertia particles in turbulent flows. Furthermore, the DIM was incorporated into the nuclear/industrial computational fluid dynamics (CFD) code SATURNE for calculating the deposition of aerosols (see¹²).

Thanks to significant progress achieved in CFD, and in particular in the development of

sophisticated turbulence models and numerical methods for unstructured grids for complex geometry, the CFD approach has been used to study the deposition of heavy particles in both simple and complex flows and geometries. This is usually carried out in an Eulerian-Lagrangian framework where individual particles are tracked through a random Eulerian flow field in which the mean flow, the timescales and rms of the velocity fluctuations are based on a solution of a closed set of Reynolds-Averaged Navier-Stokes (RANS) equations for the underlying carrier flow field. To obtain statistically significant results it is necessary to carry out the calculation for a huge amount of particles, each particle associated with a particular realization of the random flow field. This facility has been embedded into most CFD codes, although the stochastic nature of both the turbulence of the underlying flow and the dispersed particulate flow makes the problem of turbulent dispersed particulate flows more complex than its single-phase counterpart. Therefore, in order to acquire as accurate as possible numerical predictions on turbulent particle deposition, additional modelling work is needed to be incorporated into the RANS equations modelling framework to account for the effect of turbulence on the dispersion of particulate phase. Furthermore, the value of the modelling is needed to be accurately assessed by comparing the results against experimental measurements or data determined by direct numerical simulation (DNS) or large eddy simulation (LES) (see^{13–19}).

There have been several investigations into ways of extending the existing basic Lagrangian particle tracking method in a RANS modelling framework for calculating particle deposition, since the default model in commercial CFD codes gives several orders of magnitude over-prediction of the particle deposition rates for very small particles. Greenfield²⁰ implemented the random eddy interaction boundary layer approach proposed by Kallio and Reeks⁶ in the CFD code CFX to study deposition of heavy particles. Similar work was performed by both Matida *et al.*²¹ and Kroer and Drossinos²² who applied the same model as Kallio and Reeks⁶ for particle deposition in a turbulent pipe flow, in which the Lagrangian time scales encountered by small particles were modified in order to match results obtained by numerical simulations with the experimental measurements of Liu and Agarwal²³. Dehbi²⁴ implemented the random eddy interaction model as user defined functions (UDFs) in ANSYS FLUENT in which the fluid velocity fluctuations encountered by particles within the turbulent boundary layer are fed in via curve fitted DNS data. The same method was employed by Horn and Schmid²⁵ to extend the Lagrangian particle tracking facility in CFX.

The essence of the work of these researchers^{20,22,24,25} has been to improve upon the detailed statistics of the turbulent boundary layer which is not properly resolved in the most-widely used standard $k - \epsilon$ turbulence model in a CFD modelling framework. A particular inadequacy is the isotropic assumption used in the standard $k - \epsilon$ model to calculate fluctuating fluid velocities $u'_i = \sqrt{2k/3}$. Associated with this is the structure and timescale of the near wall turbulence that is a critically controlling factor for the deposition of heavy particles. As well as the simple and efficient standard $k - \epsilon$ turbulence model, Tian and Ahmadi²⁶ carried out a thorough comparison of other turbulence models in particle deposition predictions. They demonstrated that the Reynolds stress model (RSM) in ANSYS FLUENT coupled with an enhanced wall treatment still gives significant over-prediction of deposition rates. Interestingly however, Parker *et al.*²⁷ using RSM but a different method of evaluating the particle deposition flux at the wall obtained very good agreement with the benchmark experimental data from Liu and Agarwal²³.

However, there is another way referred to as a continuous random walk (CRW) model which uses a Langevin equation to calculate fluid velocity fluctuations encountered along particle trajectories. Dehbi²⁸ developed a normalized Langevin equation based CRW model, which was implemented as a user defined function (UDF) in ANSYS FLUENT to account for the inhomogeneous anisotropic boundary layer turbulence. A significant advance in the use of this approach was made by Guingo and Minier²⁹ who proposed a novel one-dimensional CRW boundary layer model of the fluid fluctuating velocity which explicitly simulated the interaction of heavy particles with the near wall coherent structures (e.g. sweeps and ejections). This model was then implemented in the open source CFD code SATURNE. Similar methodology has been employed by Chibbaro and Minier³⁰ who obtained satisfactory predictions of deposition rates with the standard $k - \epsilon$ model in SATURNE. In this regard, both Guingo and Minier²⁹ and Chibbaro and Minier³⁰ demonstrated the important role played by the near wall coherent structures on the transport and deposition of heavy particles within turbulent boundary layers.

Since Kline *et al.*³¹ first reported the presence of well-organized spatially and temporally dependent motions in the near wall region (referred to as bursting) of a turbulent flow, the role played by coherent structures of near wall on the transport and deposition of inertia particle has been the focus of attention of a number of researchers before Guingo and Minier²⁹. Owen³² was the first to suggest that the transport of fine solid particles from a

turbulent gas stream to an adjoining surface may arise from sporadic violent eruptions from the viscous sublayer. Cleaver and Yates³³ proposed a sub-layer model, which takes into account the role of the up-sweeps and down-sweeps of fluid observed in the near wall region of turbulent flows, in order to obtain a better understanding of the mechanics of the particle deposition process. The model predictions were in satisfactory agreement with experimental measurements on deposition rates. The sub-layer model of Cleaver and Yates³³ was used by Fichman *et al.*³⁴ and Fan and Ahmadi³⁵ for calculating particle deposition. Wei and Willmarth³⁶ carried out a quadrant analysis of laser Dropper anemometer (LDA) measurements of near wall fluid velocity in order to acquire a preliminary understanding of suspended sediment transport. Kaftori *et al.*³⁷ and Kaftori *et al.*³⁸ demonstrated the importance of coherent wall structures on particle motion in a turbulent boundary layer and on subsequent entrainment and deposition processes via a series of systematic experiments. Marchioli and Soldati³⁹ further examined the mechanisms for particle transfer and segregation in turbulent boundary layers through DNS calculations of channel flow. They revealed that downward sweeps, referred to as quadrant IV events, cause particles to transfer to the near wall region where particle preferentially accumulate in the low-speed streaks, whilst ejections, referred to as quadrant II events bring about the migration of particles to the region of outer flow. Soldati and Marchioli⁴⁰ provided a systematic review and physical insight into the physics and modelling of deposition and entrainment of particles from turbulent flows. It has been the source of better implementation of models for particle depositions in practical simulation scenarios.

The work of Wei and Willmarth³⁶ has been particularly important in developing and implementing the methodology for calculating the particle transport in a turbulent boundary layer proposed in this paper. They performed the quadrant analysis of Willmarth and Lu¹ to examine the high-resolution, two-component laser-Doppler anemometer measurements of the wall normal fluid velocity fluctuations in a fully developed water channel flow. They found that there is a net upward momentum flux in the range of $y^+ > 30$ that may be associated with the bursting process occurring in quadrant II, whilst there is a net downward momentum flux in the range of $10 \leq y^+ \leq 30$ that may be associated with the sweeps process occurring in quadrant IV. The net momentum flux results from the positively skewed distribution of the fluctuating wall-normal velocity. Inspired by this approach, the present work proposes another way to model near wall coherent structures and their interaction with

particles under a positively skewed distribution of wall-normal fluctuating velocities.

In formulating and examining this approach, this paper is structured as follows. First, the stochastic quadrant model is formulated and discussed. We then present the statistics in the four quadrants obtained using a quadrant analysis of the wall-normal fluid velocity fluctuations acquired from an LES of a fully developed channel flow. Finally, results for the deposition rates from an implementation of this stochastic quadrant model are presented and compared with results from benchmark experimental measurements, and those obtained from a one-dimensional Langevin equation-based CRW model and other CRW models. Several statistics concerning the transported particles in the near wall region are also shown.

II. MODELLING METHODOLOGY

A. Formulation of the stochastic quadrant model

The discrete random walk (also known as Monte-Carlo eddy interaction) model is the basis of the formulation of the present stochastic model. The fluid velocity field in the absence of the dispersed particle phase is determined by a RANS computation with the standard $k - \epsilon$ model (see⁴¹). The temporal fluctuations of the velocity field are described by a sequence of discrete eddies, with which the suspended particles interact for a randomized eddy lifetime. In the particle equation of motion, the instantaneous fluid velocity is represented by a Reynolds decomposition of averaged and fluctuating components, $\mathbf{u} = \bar{\mathbf{U}} + \mathbf{u}'$. The time-averaged fluid velocity $\bar{\mathbf{U}}$ is acquired from the solution of a RANS calculation for the turbulent flow. Thus it is crucial to model the fluctuating components to account for the effect of turbulence on the dispersion of particles. In this respect, there have been a number of attempts that we have referred to in the introduction (see also^{24,26,28–30,42}).

In this work, our attention is confined to the turbulent deposition of particles onto perfectly absorbing adjacent surfaces in a fully developed turbulent boundary layer, in which the flow velocity statistics are independent of streamwise coordinate x . As stated by Pope⁴³, a fully developed channel flow can be considered as statistically stationary and one-dimensional, with velocity statistics depending on the wall normal direction y only. In this case, a new approach is proposed here to model the wall-normal fluctuating velocity component denoted by v' based on quadrant analysis of the coupled (v', u') Reynolds shear stress

domain. In addition, the particle tracking is performed using a Lagrangian particle tracking module independent of the discrete phase model (DPM) provided by ANSYS FLUENT.

It is widely considered that the distribution of the wall normal fluctuating velocity is skewed within fully developed turbulent boundary layers (see⁴⁴). The wall normal fluctuating velocity component v' can be distinguished as positive or negative according to whether the momentum flux is away from or towards the wall. Thus let v'_+ be a function defined as

$$v'_+ = \begin{cases} v' & \text{if } v' > 0, \\ 0 & \text{if } v' \leq 0 \end{cases} \quad (1)$$

and v'_- defined as

$$v'_- = \begin{cases} v' & \text{if } v' < 0, \\ 0 & \text{if } v' \geq 0. \end{cases} \quad (2)$$

It is possible to define the average value of v'_+ and v'_- as: $\langle v'_+ \rangle = \frac{1}{T_+} \int_0^T v'_+ dt$ and $\langle v'_- \rangle = \frac{1}{T_-} \int_0^T v'_- dt$, where T is the interval of observation time containing the fraction of v'_+ denoted by T_+ and the fraction of v'_- denoted by T_- . We then have $\langle v'_+ \rangle + \langle v'_- \rangle = \frac{1}{T} \int_0^T (v'_+ + v'_-) dt$. Accordingly,

$$\frac{1}{T} \int_0^T (v'_+ + v'_-) dt = 0. \quad (3)$$

Thus if $T_+ < T_-$,

$$|\langle v'_+ \rangle| > |\langle v'_- \rangle|, \quad (4)$$

if $T_+ > T_-$,

$$|\langle v'_+ \rangle| < |\langle v'_- \rangle|. \quad (5)$$

Similarly, average momentum flux per unit area can be defined as:

$$\langle v'^2_+ \rangle = \frac{1}{T_+} \int_0^T (v'_+)^2 dt \quad (6)$$

and

$$\langle v'^2_- \rangle = \frac{1}{T_-} \int_0^T (v'_-)^2 dt. \quad (7)$$

According to Eq: (4), when $T_+ < T_-$ we have

$$\left| \langle v'^2_+ \rangle \right| > \left| \langle v'^2_- \rangle \right|, \quad (8)$$

and according to Eq: (5), when $T_+ > T_-$

$$\left| \langle v'^2_+ \rangle \right| < \left| \langle v'^2_- \rangle \right|. \quad (9)$$

It is obvious that $|\langle v'^3_+ \rangle| > |\langle v'^3_- \rangle|$ when $T_+ < T_-$; whilst $|\langle v'^3_+ \rangle| < |\langle v'^3_- \rangle|$ when $T_+ > T_-$. These two cases mean that the wall normal fluctuating component is derived from positively and negatively skewed distributions, respectively. Under the positively skewed distribution, there will be a net upward momentum flux of fluid; whilst under the negatively skewed distribution, there will be a net downward momentum flux of fluid. This imbalance of momentum flux of fluid particle within fully turbulent boundary layers could play an important role on the transport and deposition of heavy particles. The data from Kim *et al.*⁴⁴ show that the wall normal fluctuating component is of positive skewness in the range of $0 < y^+ < 10$ and $y^+ > 30$.

B. Statistics of v' in each of the four quadrants

Following the quadrant analysis approach of Willmarth and Lu¹ for analysing the structure of the Reynolds stresses, we classified the wall normal fluctuating velocity and averaged it in the four quadrants according to the instantaneous flow velocity in the quadrant domain. In this sense, the instantaneous velocity of a sufficiently large number of fluid particles at a specified position may be categorized in terms of the sign of the streamwise and wall normal velocity fluctuations. For example, when both u' and $v' > 0$ the instantaneous velocity signal is allocated to quadrant I (Q_I); in the case of $u' < 0$ and $v' > 0$, it is allocated in quadrant II (Q_{II}); when both u' and $v' < 0$, is allocated to the quadrant III (Q_{III}); finally, if $u' > 0$ and $v' < 0$, it is allocated to quadrant IV (Q_{IV}). We note that upward momentum fluxes may be associated primarily with the bursting process associated with events in Q_{II} , whilst downward momentum fluxes are associated with sweep events in Q_{IV} . Physically speaking, upward momentum fluxes associated with Q_{II} would cause particles to move away from the wall and downward momentum fluxes associated with Q_{IV} would result in the migration of particles toward the wall.

Time averages of v' and momentum flux v'^2 can be defined for each of the four quadrants according to Eq: 4 and 6 as

$$\langle v'_i \rangle = \frac{1}{T_i} \int_0^T v'_i dt; \quad i = \text{I, II, III, IV} \quad (10)$$

and

$$\langle v'^2_i \rangle = \frac{1}{T_i} \int_0^T v'^2_i dt; \quad i = \text{I, II, III, IV}, \quad (11)$$

where T_i denotes time spell spent in the quadrant i by v'_i , and v'_i is define as

$$v'_i = \begin{cases} v' & \text{if } v' \text{ satisfies the criterion of quadrant analysis,} \\ 0 & \text{if not.} \end{cases} \quad (12)$$

A large eddy simulation (LES) of a fully developed channel flow with $Re_\tau = 180$ was carried out to obtain the corresponding statistics of v'_i up to $y^+ = 100$. The LES was based on a dynamic Smagorinsky sub-grid scale (SGS) model⁴⁵ and a generalized fractional-step method⁴⁶ for the overall time-advancement. A scatter plot of u' and v' together with the corresponding probability density function (pdf) (based on 162000 non-dimensional time units) is shown in FIG. 1 according to the quadrant analysis (a schematic graph of the quadrant analysis is shown in Guingo and Minier²⁹). We note that the probability density functions of u' and v' are skewed.

In FIG. 2, the quadrant mean $\langle v'_i \rangle$ and wall normal flow velocity rms $\langle v'^2 \rangle^{1/2}$ as a function of y^+ show that the fluctuating components in the four quadrants are smaller in magnitude than the wall normal flow velocity rms $\langle v'^2 \rangle^{1/2}$ across the y^+ range shown. $\langle v'_i \rangle$ in each of the four quadrants is of different magnitude, indicating that there is an asymmetry in the wall normal fluctuating components. Furthermore, the greatest magnitude of $\langle v'_i \rangle$ is found in Q_{II} across most of the y^+ range. FIG. 3 shows that there is a net upward momentum flux resulting from Q_{II} for the range of $y^+ > 20$. However, this situation is reversed in the range of $y^+ < 20$. The asymmetry of $\langle v'_i \rangle$ and $\langle v'^2_i \rangle$ in each of the four quadrants is a new feature for modelling velocity fluctuations encountered by heavy particles, which we believe is particularly useful for measuring particle transport and deposition in the near wall region.

C. Implementation of the stochastic quadrant model

The imbalance of $\langle v'_i \rangle$ within each of the four quadrants will be of differing importance to the transport and deposition of heavy particles. Events in quadrant II are mainly associated

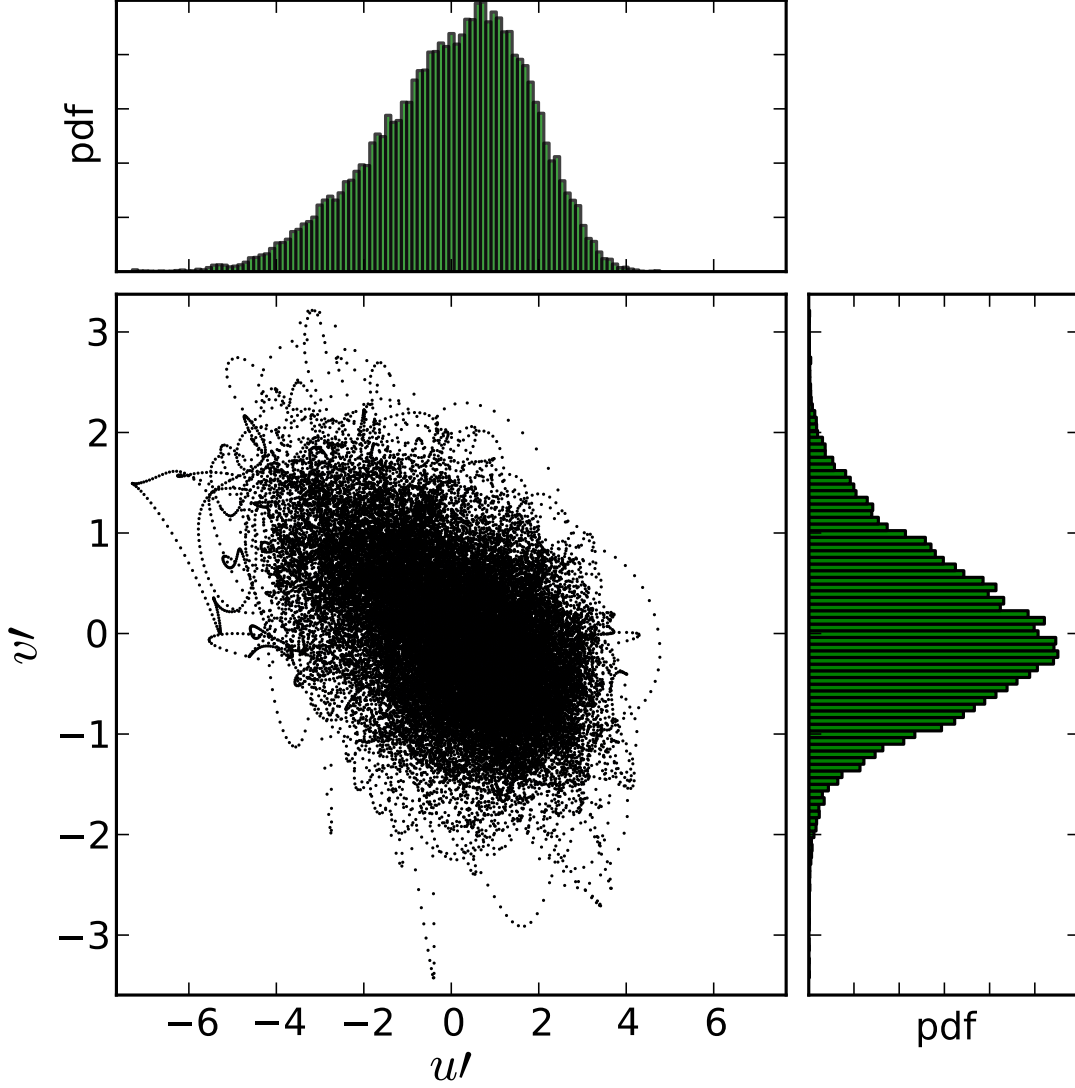


FIG. 1: Scatter plot of u' and v' at $y^+ = 50$ resolved by LES, categorised in terms of quadrant analysis.

with violent ejections of low-speed fluid away from the wall; motions in quadrant IV are primarily associated with an inrush of high-speed fluid toward the wall, also referred to as the sweeping event. There are no significant structures associated with quadrant I and III. The upward momentum flux in quadrant II may be a strongly contributing factor on the transport of particles away from the wall and reduce the deposition rates; whilst the inward momentum flux in quadrant IV may be a strongly contributing factor on the transport of

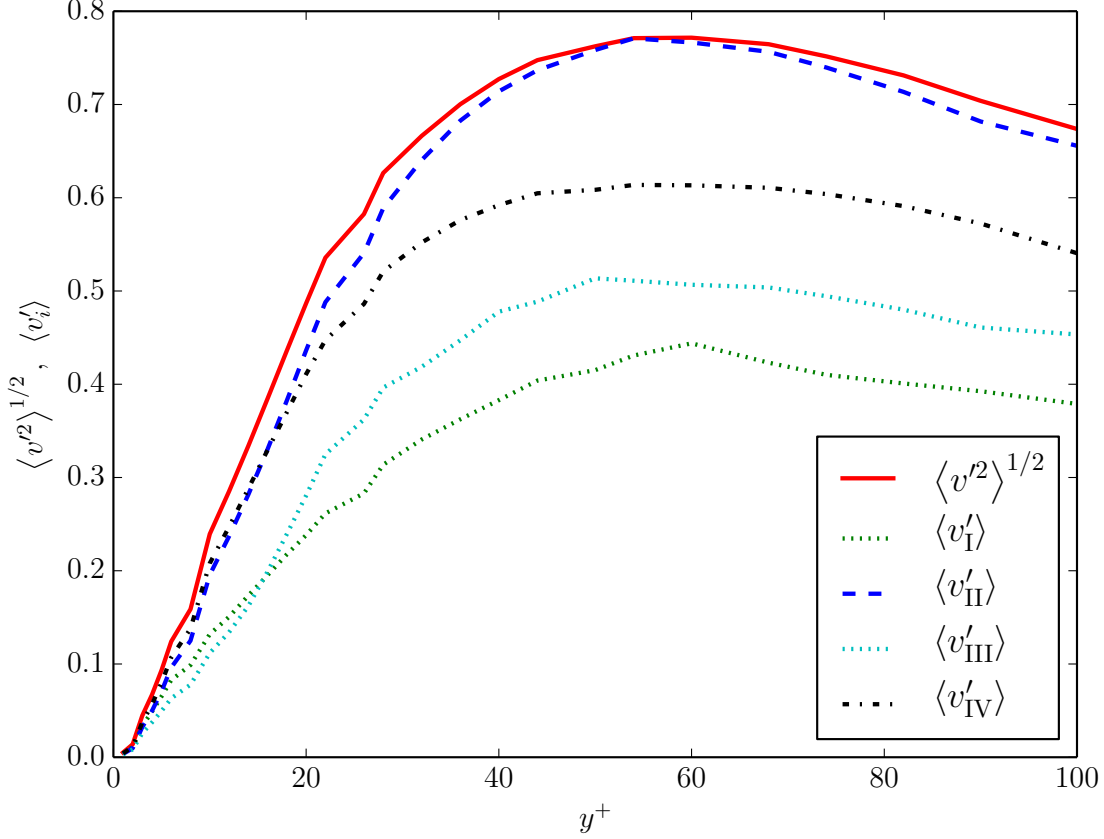


FIG. 2: Profiles of $\langle v'^2 \rangle^{1/2}$ and $\langle v'_i \rangle$ as a function of y^+ at $Re_\tau = 180$ in each of the four quadrants.

particles towards the wall and increase the deposition rates.

The results on $\langle v'_i \rangle$ and $\langle v'^2 \rangle$ enables us to specify the statistics of wall-normal velocity fluctuations encountered by particles in each eddy along their trajectories. For example, curve-fitting of the four profiles of $\langle v'_i \rangle$ could be achieved easily. However, comparing the shape of $\langle v'_i \rangle$ with the shape of $\langle v'^2 \rangle^{1/2}$, a different scale factor is assumed between $\langle v'_i \rangle$ and $\langle v'^2 \rangle^{1/2}$. In FIG. 4 the probability density functions for a half normal distribution for v'_i in each of the four quadrants at $y^+ = 30$ shows that they are in fair agreement with each other, indicating that a half normal distribution may be used to describe the distribution of v'_i . This probability distribution function is given by

$$f_X(x; \sigma) = \begin{cases} \frac{\sqrt{2}}{\sigma\sqrt{\pi}} \exp\left(-\frac{x^2}{2\sigma^2}\right) & \text{if } x \geq 0, \\ 0 & \text{if } x < 0, \end{cases} \quad (13)$$

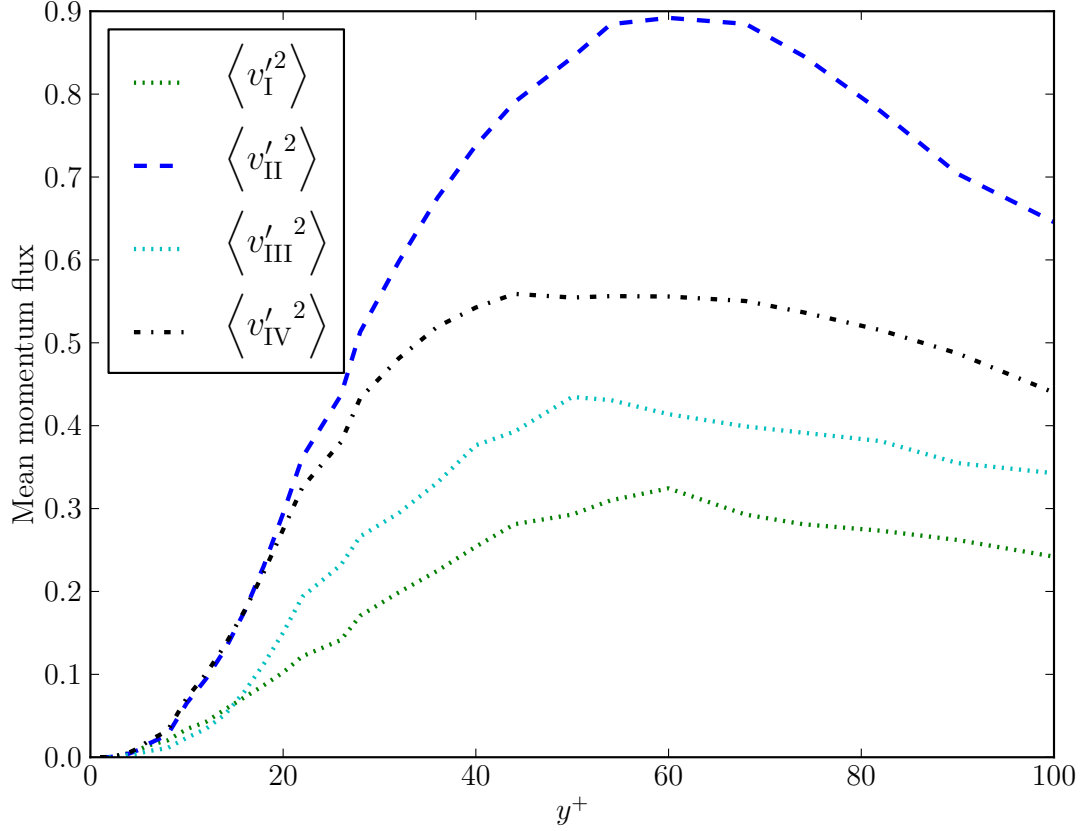


FIG. 3: Profiles of momentum fluxes as a function of y^+ at $Re_\tau = 180$ in each of the four quadrants.

where σ is set to equal to the value of $\sqrt{\frac{\pi}{2}} \langle v_i'^2 \rangle^{1/2}$ at the corresponding y^+ location.

The logical next step is to construct a random process, which models the eddy motions in the four quadrants. Particles will interact with a random succession of eddies resulting from different quadrants. For this, a homogeneous Markov chain was conceived as a model for the evolution of eddy events in the four quadrants along the particle trajectories. Particles may interact with an eddy in quadrant I. After this eddy decays, they would then be able to interact with an eddy resulting from any of the four quadrants with a certain transition probability. FIG. 5 describes this process.

As far as the transition probabilities are concerned, let $Q_i, i = \{I, II, III, IV\}$ be a discrete time Markov chain on $\{Q_I, Q_{II}, Q_{III}, Q_{IV}\}$ with a transition matrix

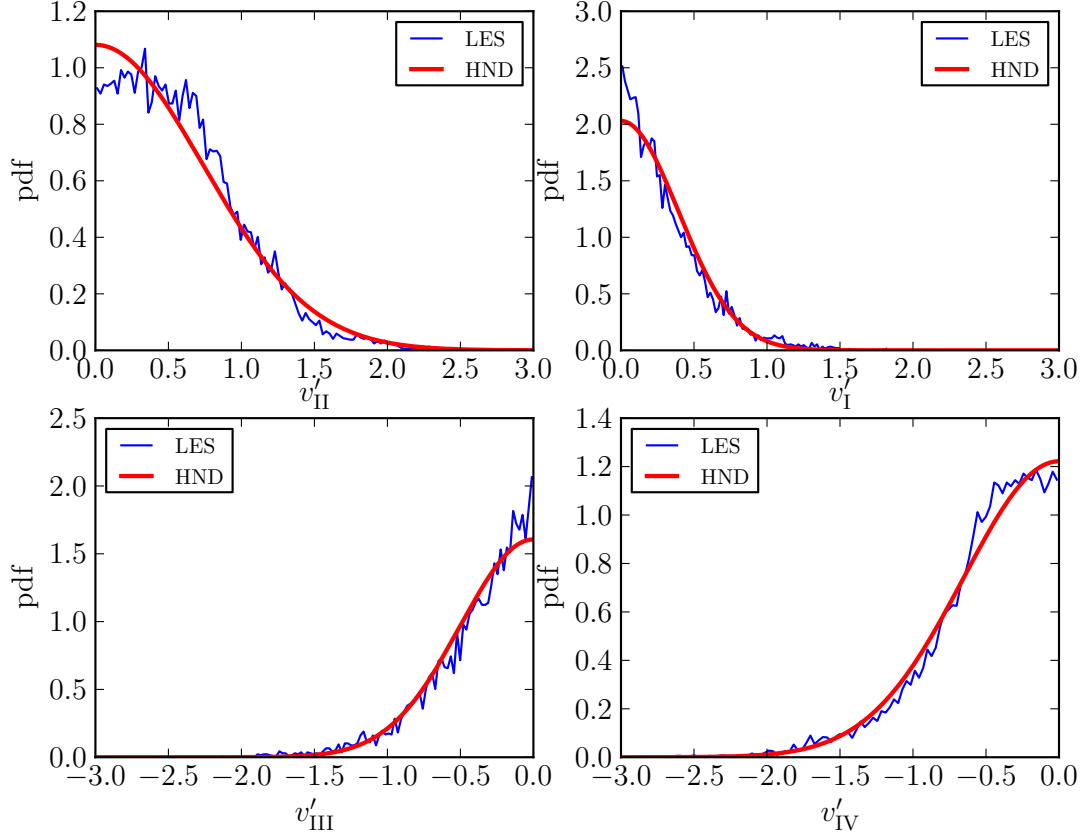


FIG. 4: Probability density function (pdf) for v'_i obtained by LES and a comparison with a half normal distribution (HND)

$$P = \begin{pmatrix} p_{11} & p_{12} & p_{13} & p_{14} \\ p_{21} & p_{22} & p_{23} & p_{24} \\ p_{31} & p_{32} & p_{33} & p_{34} \\ p_{41} & p_{42} & p_{43} & p_{44} \end{pmatrix}, \quad (14)$$

where $(p_{ij} : i, j \in \{1, 2, 3, 4\})$ denotes the corresponding probability distribution of random eddy events in each quadrant. The transition matrix in Eq: 14, needs to satisfy the condition $\sum_j p_{ij} = 1$. For eddy events in the four quadrants, Eq: 14 is reduced to a “degenerate” transition matrix as

$$P = \begin{pmatrix} p_{11} & p_{22} & p_{33} & p_{44} \end{pmatrix}. \quad (15)$$

FIG. 6 shows variations of the relative probability associated with each of the four quad-

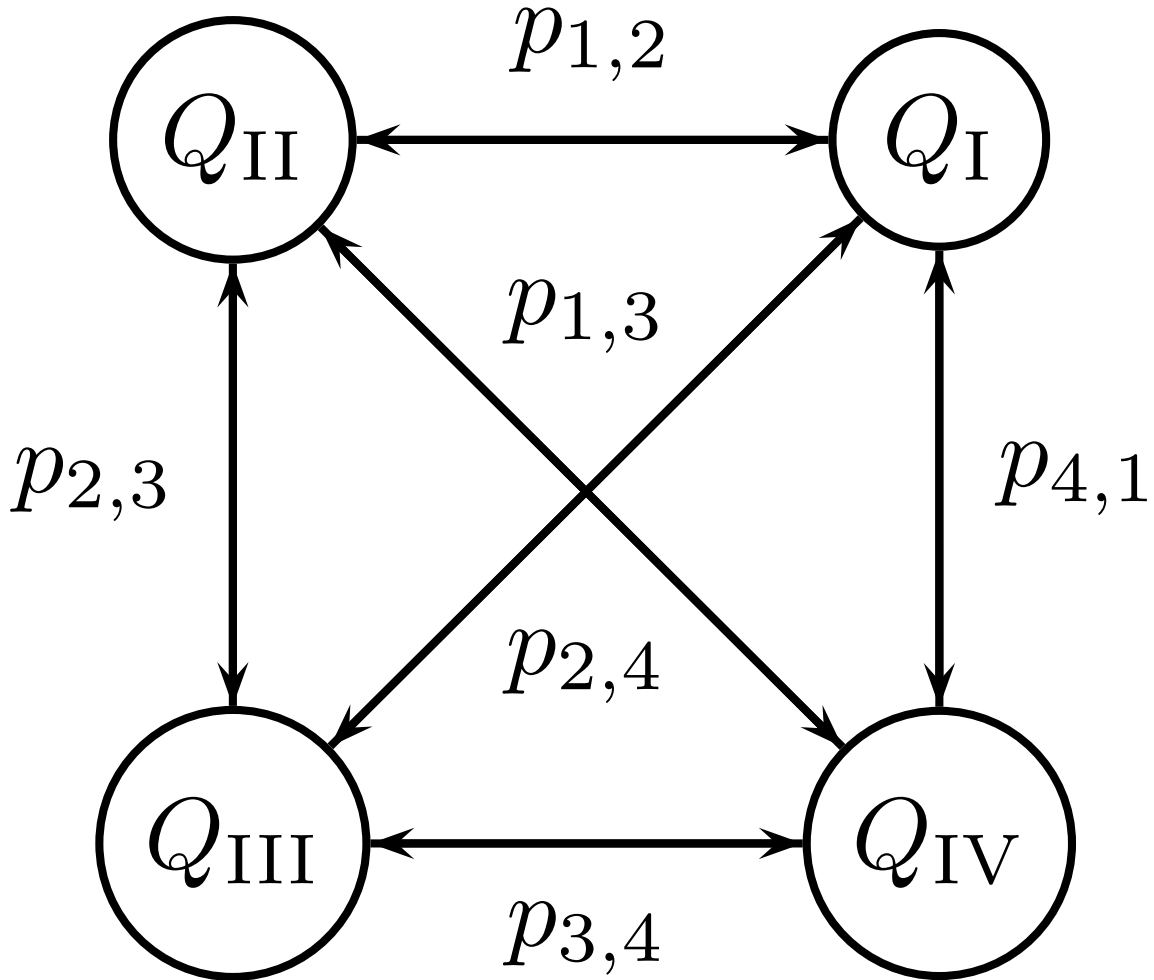


FIG. 5: Diagram describing the Markov chain modelling motions in the four quadrants.

rants as a function of y^+ . These probabilities are used as the transition probabilities denoted in Eq: (15).

The time scale of eddies in each of the four quadrants is difficult to estimate accurately from the present study, although Luchik and Tiederman⁴⁷ provided several quantitative techniques to measure time scales associated with bursting events. In the present study, the lifetime of eddies in the four quadrants are assumed to equal to the Lagrangian time scale of fluid particles according to their corresponding y^+ position. FIG. 7 shows the Lagrangian time scale of fluid particles within turbulent boundary layers. This is taken from the curve-

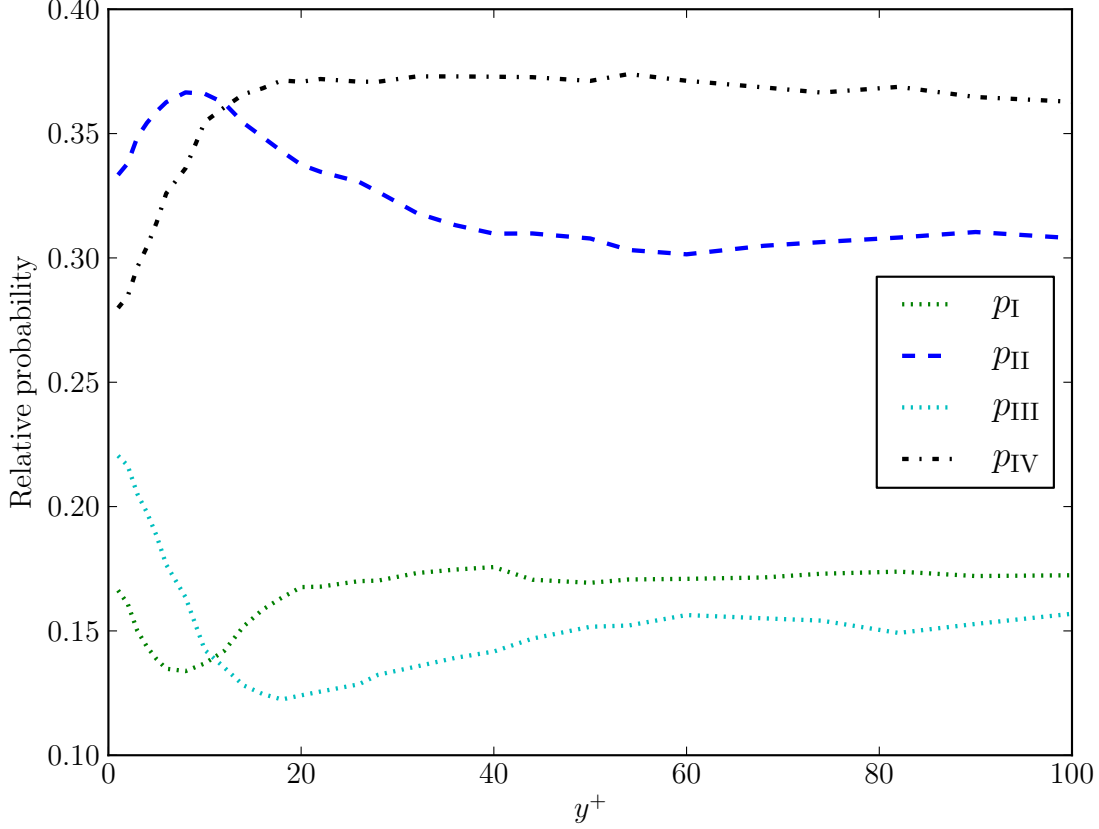


FIG. 6: Relative probability of four quadrants as a function of y^+ .

fitting of Kallio and Reeks⁶. Furthermore, the Lagrangian time scale is assumed to obey an exponential distribution

$$f_X(x, \lambda) = \lambda e^{-\lambda x}, \quad (16)$$

where λ equals the integral Lagrangian time scale T_L at the particle position. FIG. 7 also shows the wall-normal rms profile of fluid velocity. $\langle v'_i \rangle$ in each of the four quadrants is obtained by multiplying $\langle v'^2 \rangle^{1/2}$ by a scaling factor that is the ratio of the magnitude of the velocity fluctuation in each of the four quadrants to the magnitude of wall-normal velocity fluctuation. In every eddy generated in the four quadrants, the fluctuating velocity is sampled from a half normal distribution with a mean $\langle v'_i \rangle$ and a variance corresponding to the particular particle y^+ value in the boundary layer.

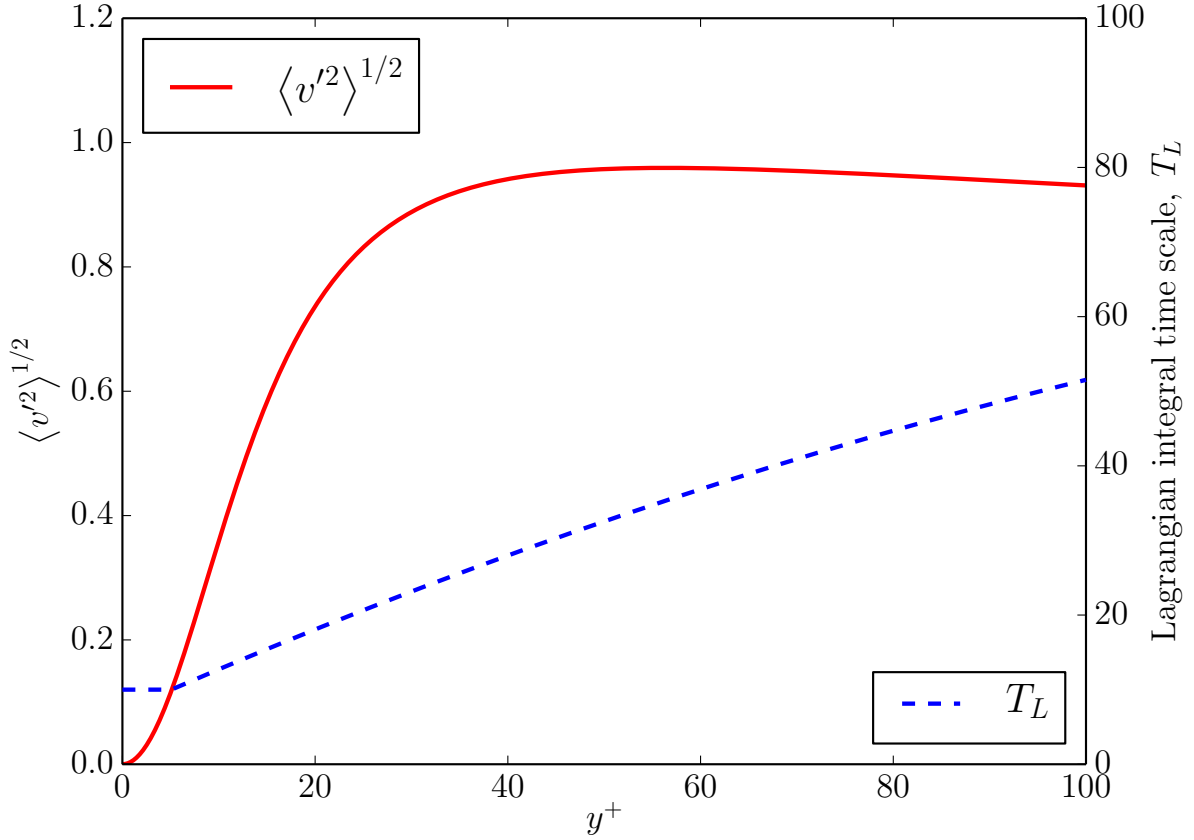


FIG. 7: Non-dimensional wall normal fluid velocity and Lagrangian time integral time scale as a function of y^+ within turbulent boundary layers.

D. Governing equations of particle motion

A Lagrangian particle tracking module was developed and coupled with the unstructured mesh Navier-Stokes equation solver in ANSYS FLUENT to calculate trajectories of heavy particles in flow fields. The focus of this work is on the deposition of non-inter-collision, rigid, spherical and heavy particles. The ratio of particles density to fluid density is 770, which is the same as the experimental measurements of Liu and Agarwal²³. The concentration of particles is dilute enough to assume one-way coupling. The particle equation of motion discussed by Maxey and Riley⁴⁸ is simplified in this work by taking into account only the drag force. We thus can write the particle equation of motion involving the non-linear form

of the drag law with the point particle approximation

$$\frac{d\mathbf{u}_p}{dt} = \frac{1}{\tau_p} C_D \frac{Re_p}{24} (\mathbf{u} - \mathbf{u}_p), \quad (17)$$

where \mathbf{u}_p is the particle velocity and \mathbf{u} the instantaneous fluid velocity at the particle position, τ_p is the particle response time. Previous research effort on particle dispersion in a turbulent channel flow (see⁴⁹) has demonstrated that the particle Reynolds number, $Re_p = |\mathbf{u} - \mathbf{u}_p|d_p/\nu$ does not necessarily remain small enough. Thus, an empirical relation for C_D from Morsi and Alexander⁵⁰, which is applicable to a wide range of particle Reynolds number with sufficiently high accuracy, is employed, namely

$$C_D = c_1 + \frac{c_2}{Re_p} + \frac{c_3}{Re_p^2}, \quad (18)$$

in which c_1, c_2, c_3 are constants and provided by Morsi and Alexander⁵⁰. The above empirical expression exhibits the correct asymptotic behavior at low as well as high values of Re_p . A state-of-art composite correlation for drag coefficient and lift coefficient will be investigated in the following work.

The position \mathbf{x}_p of particles is obtained from the kinematic relationship

$$\frac{d\mathbf{x}_p}{dt} = \mathbf{u}_p. \quad (19)$$

The boundary condition for the above equation is that the particle is captured by the wall when its center is less than its radius away from the nearest wall. This is not properly treated in the default discrete phase model (DPM) provided by ANSYS FLUENT. Furthermore, this error has a significant effect upon predictions for the deposition of heavy particles under investigation. Moreover, it is worth pointing out that the present stochastic quadrant model does not take into account the effect of build-up of deposited particles on the incoming particles. The particle capture is assumed to be perfectly absorbing with no subsequent re-suspension.

From a converged RANS computation of the velocity flow field, Eq: (19) is integrated in time using the second-order Adams-Bashforth scheme to obtain particle trajectories, whilst Eq: (17) is integrated with the second-order accurate Gear2 (backward differentiation formulae) scheme to obtain instantaneous velocity of particles. Fluid velocities solved by CFD are stored at the centroid of cells. Since it is only by chance that a particle coincides with the cell centroid, a quadratic scheme based on velocity gradient reconstruction is used

to interpolate the fluid velocity to the particle location. The collective statistical properties of the particle phase are obtained by following the trajectories of 10^5 particles.

III. RESULTS AND DISCUSSION

A. Continuous phase

The turbulent boundary layer was resolved using the standard $k - \epsilon$ model with enhanced wall treatment in ANSYS FLUENT. The y^+ value of the first cell adjacent to the wall was set at $y^+ = 1$. Two points need to be made here. First, there is no discernible discrepancy between the inlet and middle plane velocity profiles. Second, the calculated velocity profiles showed reasonable agreement with the DNS data of Kim *et al.*⁴⁴ across the boundary layer. Given the fact that RANS was employed, the small difference between the calculated and DNS values shown in FIG. 8 is reasonable. As far as there is no discrepancy between the velocity profiles from two planes, this was achieved through a special treatment for the inlet boundary condition. An auxiliary simulation was set up in a small computation domain. Then a converged velocity profile from the middle plane of this auxiliary simulation was exported to provide the initial velocity condition onto the inlet plane of a fully developed turbulent boundary layer. Through this technique, a transient region from the inlet plane is avoided.

B. Dispersed particle phase

1. Particle deposition rates

The particle deposition rate in a turbulent boundary layer is usually quantified through a mass transfer coefficient K defined as

$$K = \frac{J_w}{\bar{c}}, \quad (20)$$

where J_w represents the particle flux onto the wall surface per unit area and time and \bar{c} is the average particle concentration within the boundary layer. The computation technique proposed by Kallio and Reeks⁶ was used to calculate the non-dimensional particle deposition

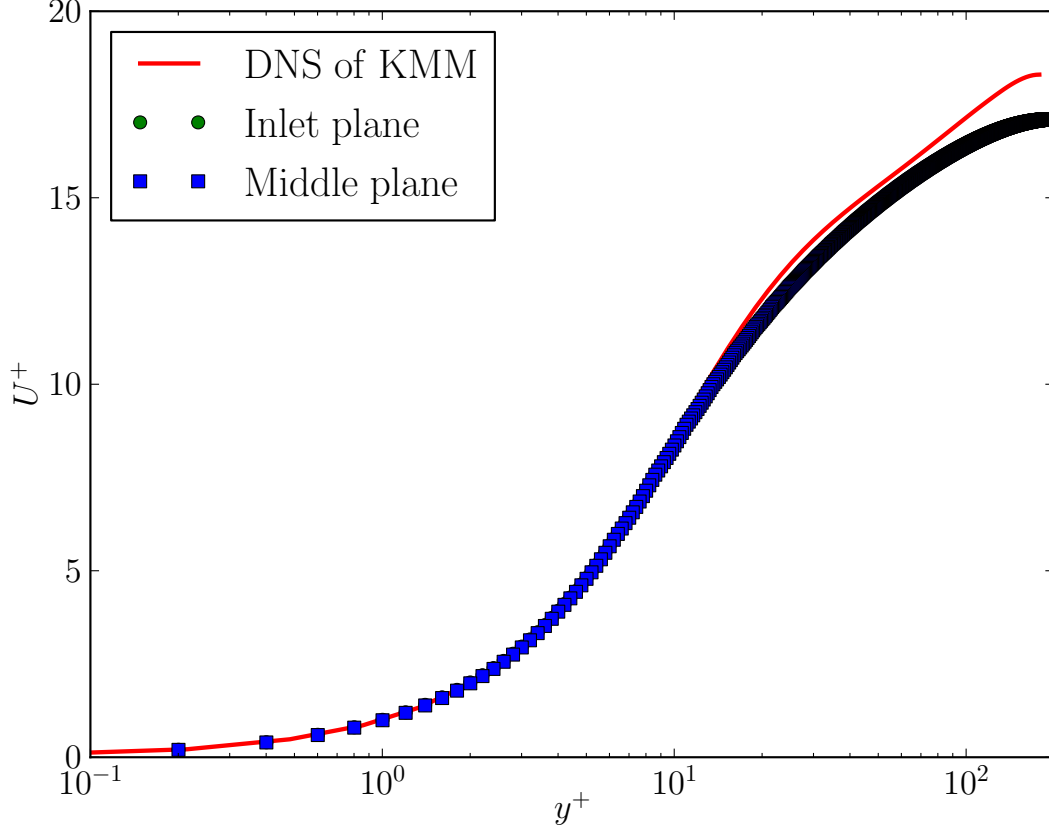


FIG. 8: Mean fluid velocity profiles from the inlet and middle plane.

velocity defined as

$$V_{dep}^+ = \frac{\bar{U}A}{u_\tau P \Delta x} \ln \left(\frac{N_{in}}{N_{out}} \right) \quad (21)$$

where \bar{U} is the average streamwise fluid velocity across the fully developed turbulent boundary layer, A is the boundary layer cross sectional area, P the duct perimeter, Δx is the incremental length of section considered, and N_{in} and N_{out} are the total number of particles passing through the start and end plane of each section, respectively. The characteristic wall friction velocity u_τ was used to obtain the non-dimensional deposition velocity V_{dep}^+ . In this study, 10^5 particles are introduced uniformly from the inlet plane.

Computed dimensionless particle deposition velocities are compared with the benchmark experimental measurements (see²³), the empirical curve-fit of McCoy and Hanratty⁵¹ and the deposition velocities predicted by the standard $k - \epsilon$ model in FIG. 9. We have also included for comparison the results from Guingo and Minier²⁹, who developed a sophisticated

stochastic model to account for the geometrical structures in turbulent boundary layers and which like the current model accounts for the influence of sweeping and ejection events. It can be observed that very good agreement exists between the present computed results and experimental data in the range of $St > 5$. For $St < 5$, the stochastic quadrant model gives an under-prediction of the deposition rates. These are also features of the stochastic model of Guingo and Minier²⁹ who predicted less deposition than obtained in this study. This under-prediction in both our model and that of Guingo and Minier may be directly attributable to the effects of ejection events on particle transport, causing particles to migrate away from the wall region and leading to an over predicted decrease in their deposition rate.

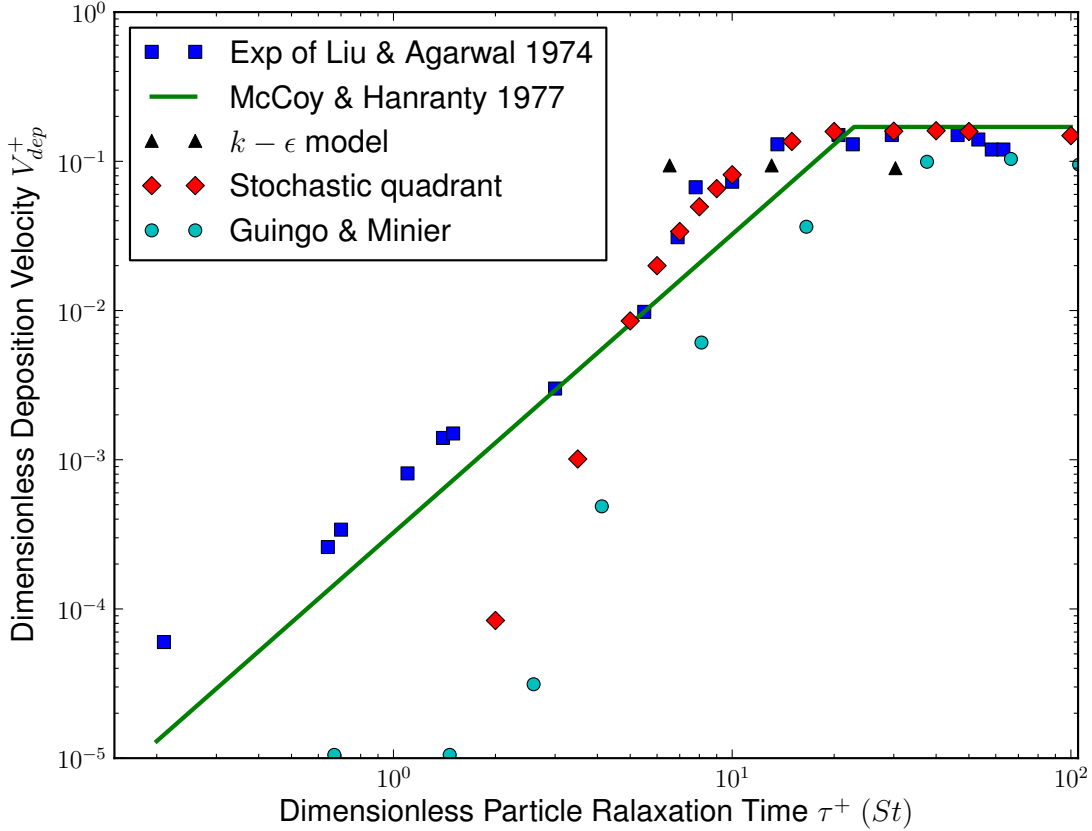


FIG. 9: Comparison of dimensionless particle deposition velocity as a function of dimensionless particle response time with experimental measurements and different models in turbulent boundary layers.

In this work, an alternative continuous random walk (CRW) model is used to repeat

the numerical study of particle deposition rates. This model is based on the wall-normal component of normalized Langevin equations in boundary layers (see^{28,52}), which takes into account the effect of Stokes number along heavy particle paths (see⁵³). The Langevin equation is solved using a second-order accuracy Milstein scheme (see⁵⁴). The non-dimensional fluctuating fluid velocity solved this way was converted to a physical velocity and then added into the particle equation of motion to account for the turbulence effect.

Results for the deposition rates from this CRW model are shown in FIG. 10. There are a few interesting points to note. Firstly, very similar results can be observed from this one-dimensional CRW model when compared to with the data of Dehbi²⁸. Secondly, the numerical results from all the models show fair agreement with experiments for large particles. However, they all give significant under-predictions on deposition rates for small particles. In contrast to the present one-dimensional CRW and stochastic quadrant model, the CRW model employed by Dehbi²⁸ was solved in three dimensions with curve-fitting DNS database. This may further corroborate the view that the wall-normal fluid fluctuations are a critical control factor on the deposition of heavy particles from fully developed turbulent boundary layer. Thus, as far as practical applications are concerned, it is possible and feasible to feed in only the wall-normal fluid fluctuations for studying particle deposition. On the other hand, compared to CRW models, the stochastic quadrant model is capable of yielding equal quality results for deposition rates, given its relatively simple nature and physical meaning of modelling the geometrical features, e.g. sweeps and ejections, explicitly in turbulent boundary layers. As a consequence, it is potentially a very promising model for studying deposition of heavy particles from turbulent flows.

Deposition rate data obtained in the previous study of Guingo and Minier²⁹, using a stochastic model to account for the coherent structures, e.g. sweeps and ejections, in turbulent boundary layers, show a good agreement with experimental data plot of Papavergos and Hedley⁵⁵ (who plotted all the available measured data on deposition rates at the time). As the present stochastic quadrant model also accounts for such features in turbulent boundary layers, it is worth comparing our predicted deposition rates with the same experimental data as Guingo and Minier have done. FIG. 11 shows the comparison. As can be seen, the predicted deposition rates from the present stochastic model fall well into the middle realm of experimental data of Papavergos and Hedley thanks to the larger scatter of the experimental data. Moreover, although the approach of the present stochastic quadrant

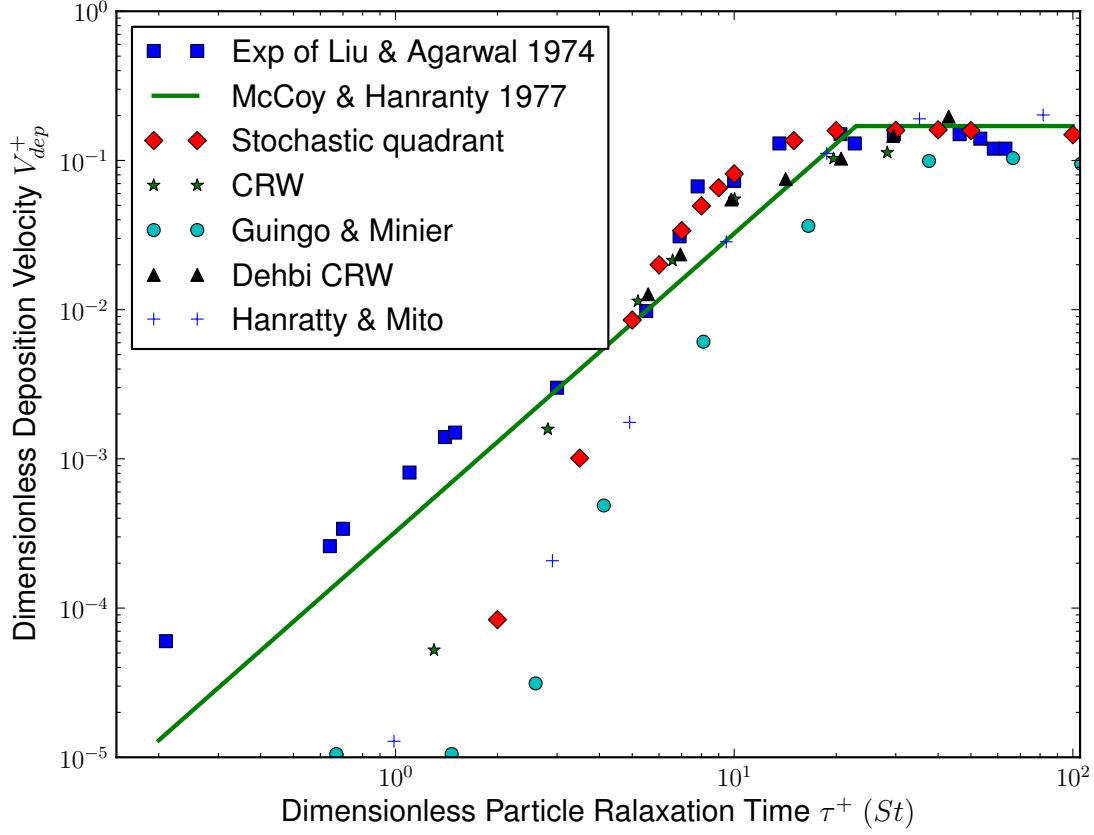


FIG. 10: Comparison of dimensionless particle deposition velocity as a function of dimensionless particle response time with experimental measurements and different models in turbulent boundary layers.

model accounting for the coherent events in turbulent boundary layers is different from that of Guingo and Minier, the predicted results for particle deposition are in line with those of Guingo and Minier.

2. Mean particle concentration

FIG. 12 shows the mean particle concentration profile as a function y^+ across the boundary layer under the assumption there is no inter-particle collisions. It can be noted that there is a significant build-up in concentration for the four classes of particles within the viscous sublayer. The phenomena of build-up of particles near the wall has been observed by numerous researchers (see^{6,18,39}) and is attributed to turbophoresis in the very near wall

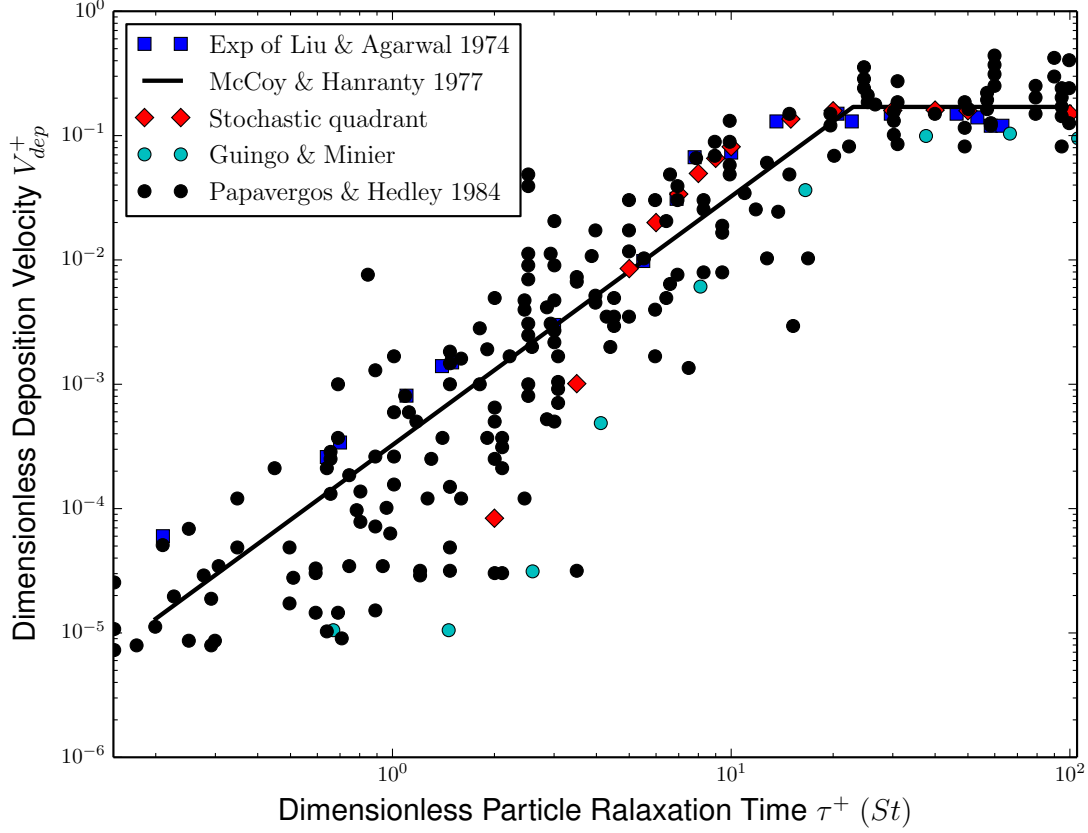


FIG. 11: Comparison of dimensionless particle deposition velocity as a function of dimensionless particle response time with experimental measurements.

region (see⁵⁶). The gradient in wall-normal fluid fluctuations in boundary layer turbulence acts as a driving force and results in a wall-ward net flux. The build-up concentration of particle with $St = 20$, is smaller than those of smaller particles with $St = 0.2, 5, 10$. This may result from the fact that particles are too heavy to follow the relatively quiescent viscous sublayer. On the other hand, they may move across the viscous sublayer and deposit on the adjacent wall surface, which may also be responsible for the relative reduction of build-up.

3. Mean wall-ward drift velocity

FIGs. 13 and 14 show the mean wall-ward drift and sampled fluid velocity profiles in the near wall region. We observe that the four sets of particles, $St = 0.2, 5, 10, 20$, have non-zero wall-ward mean velocity (negative) values. This indicates that the present

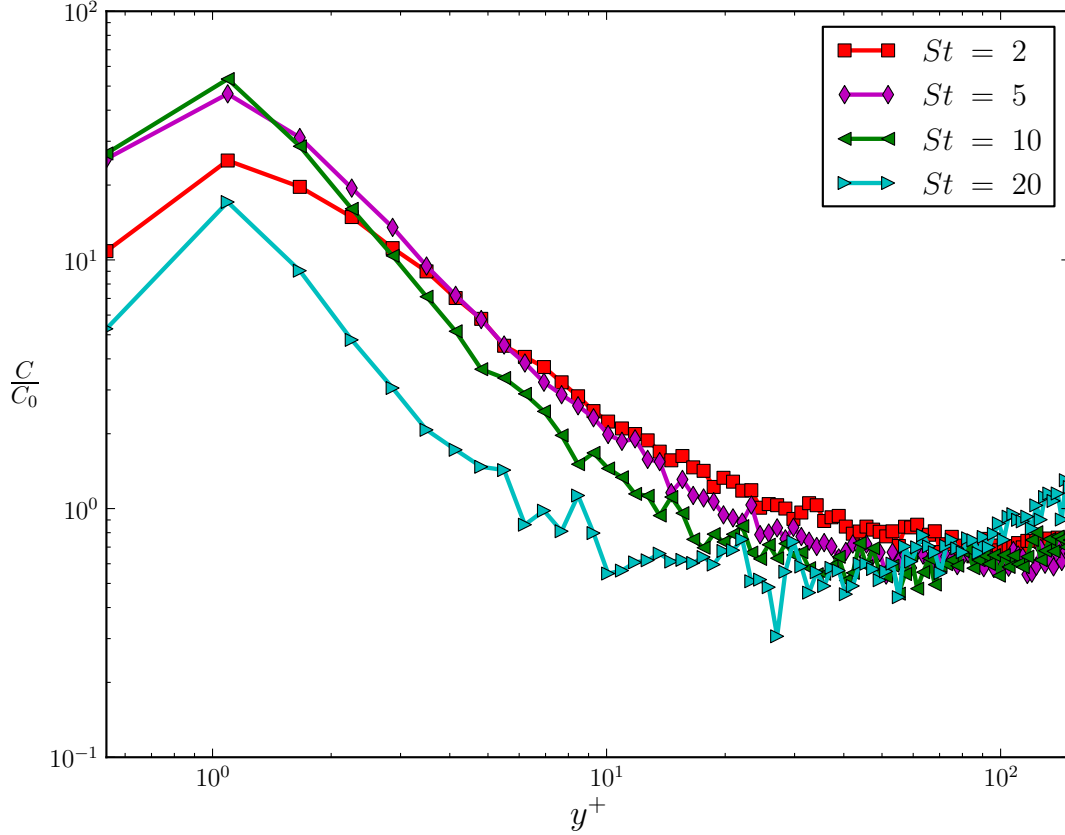
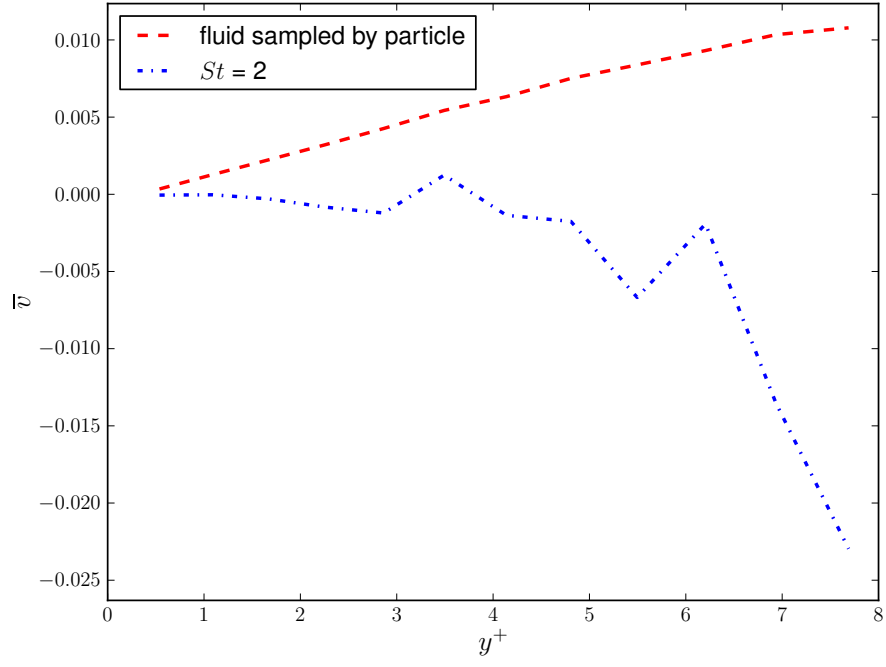


FIG. 12: Particle preferential concentration profile as a function of y^+ .

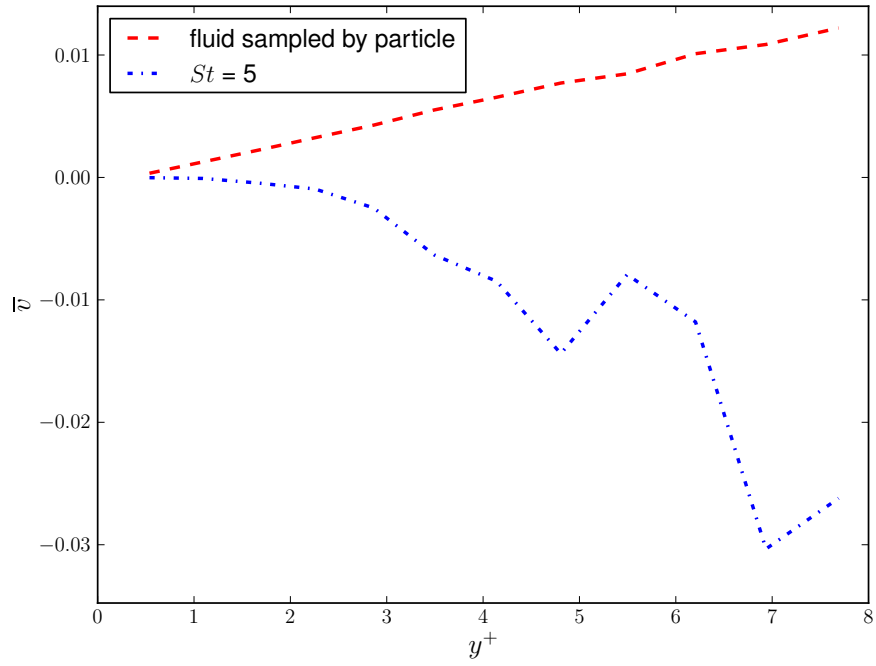
stochastic quadrant model is capable of predicting the phenomena of turbophoresis. This wall-ward mean velocity of heavy particles results primarily from the turbulence gradient of the boundary layer turbulence as well, which is the prime mechanism that is responsible for the build-up of particles. It is observed that the mean wall-ward drift velocity of particles varies monotonically with the increase of the particle inertia. Although the wall-normal fluid velocity has zero mean, the sampled mean fluid velocity at the particle location has positive values. This may result from the fact that particles preferential sample of events in quadrant II (ejections) are characterized by a large positive mean velocity. .

4. *Root mean square (rms) velocity profiles*

FIGs. 15 and 16 show the comparison of the rms of velocity fluctuations of four sets of particles with the fluid velocity fluctuations. It is observed that the r.m.s of particle phase is

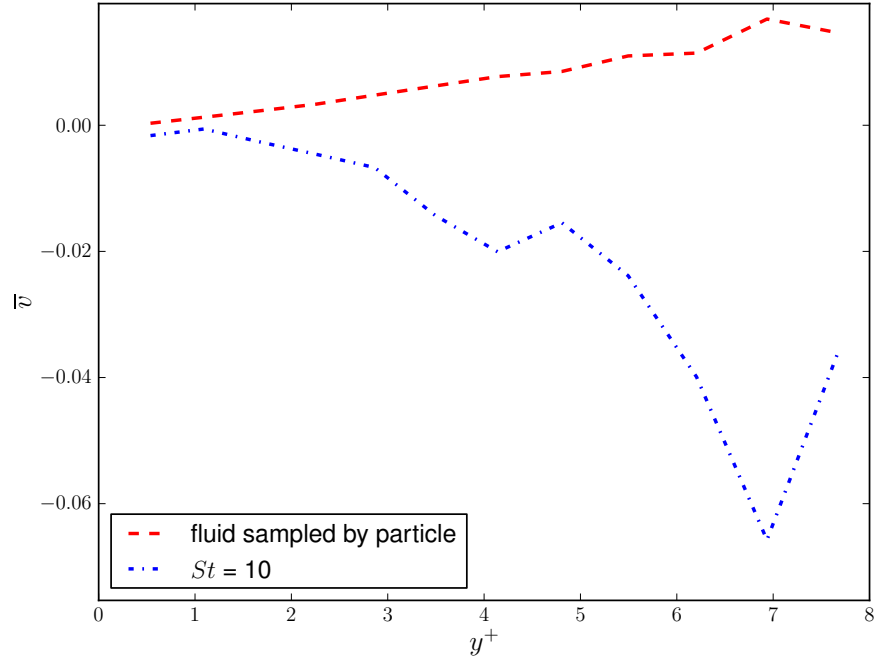


(a)

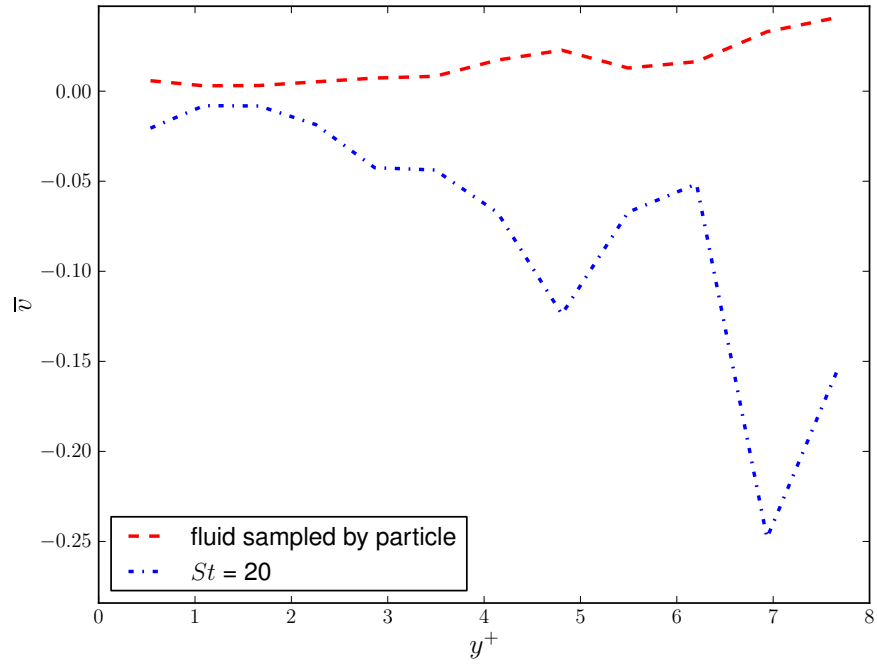


(b)

FIG. 13: Mean wallward drift velocity and sampled wall-normal fluid velocity, (a) $St = 2$,
(b) $St = 5$.



(a)



(b)

FIG. 14: Mean wallward drift velocity and sampled wall-normal fluid velocity, (a) $St = 2$,
(b) $St = 5$.

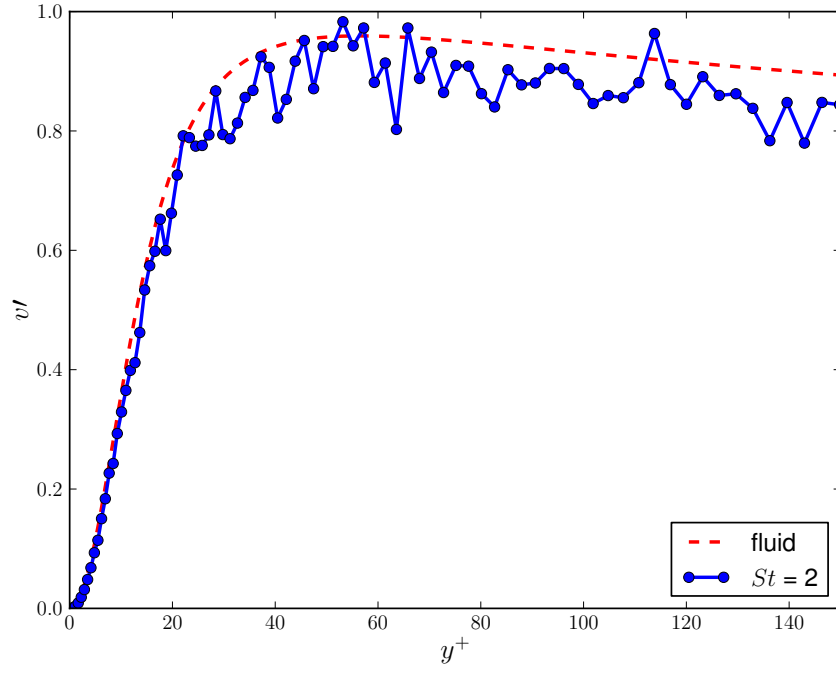
significantly different from the fluid phase. The difference increases with increasing particle inertia. This results from the fact that the heavier the particles, the slower their response to the change of surrounding fluid. As far as the raggedness displayed in the computed particle r.m.s profile is concerned, the reasons may be that the particle phase still has not reached equilibrium or that each sampling bin does not have a sufficient number of representative particles.

5. *Mechanisms for particle deposition*

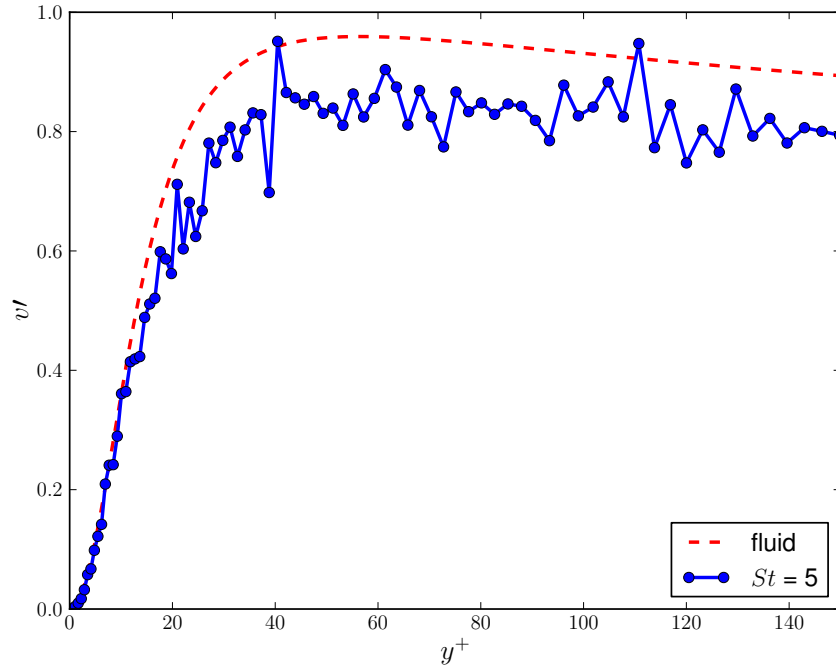
The present stochastic model has also been used to study the mechanisms for particle deposition. By analysing extensively the DNS data-sets for particle transport in turbulent boundary layers, Brooke *et al.*⁵⁷ and Narayanan *et al.*¹⁸ attributed deposition to two different mechanisms depending the particle inertia (Stokes number, St). Relatively low inertia particles deposit by a diffusion mechanism, whilst high inertia particles deposit as a result of free-flight. To differentiate between the two mechanisms, the concept of particle residence time introduced is namely the continuous time spent by a particle within a certain wall region before depositing is. Through diffusion, depositing particles have relatively smaller values of deposition velocity and larger values of residence time. Compared to the diffusion counterpart, depositing particles via free-flight mechanism have opposite values, e.g. relatively larger values of deposition velocity and smaller values of residence time. For the deposition velocities and residence time, FIG. 17 shows a scatter plot of wall-normal deposition velocities as a function of particle residence time within the region of $y^+ < 3$. The red curve is plotted according to the relation between the wall normal deposition velocity V_{dep}^+ and the residence time T_{res}^+ provided by Narayanan *et al.*¹⁸

$$V_{dep}^+ = \frac{3 - d_p^+/2}{\tau^+ \left[1 - \exp \left(\frac{T_{res}^+}{\tau^+} \right) \right]}, \quad (22)$$

where d_p is the non-dimensional particle diameter, which is based on the free-flight theory³. It can be observed that the deposited particles with $St = 2$ do not follow the free flight theory defined by Eq: 22 as they assume relatively large near-wall residence time and small deposition velocity. These particles are usually referred to as the diffusion deposition population¹⁸. For the particles with $St = 5$, there are two distinct populations of particles. The first population assumes very long near-wall residence time and negligible deposition velocity;

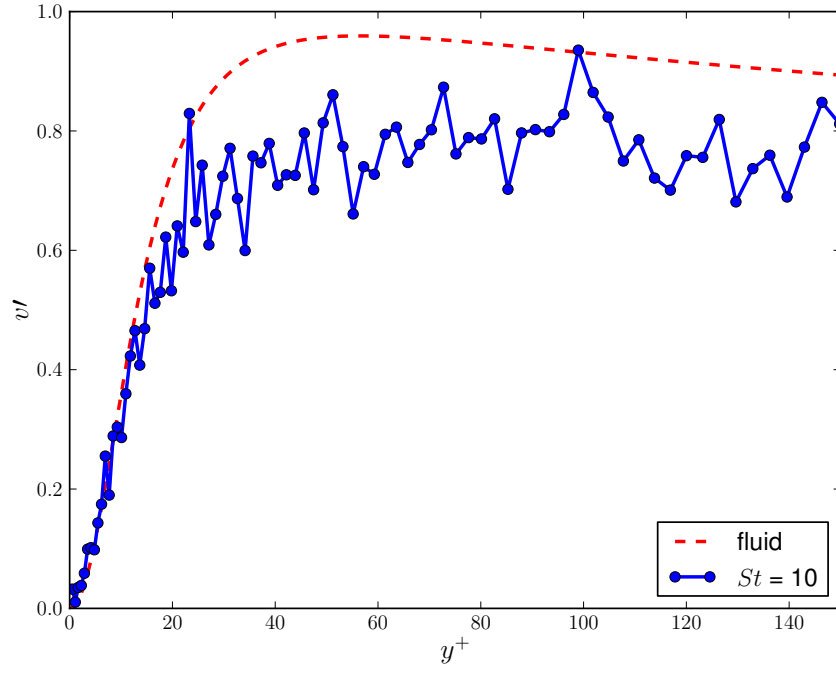


(a)

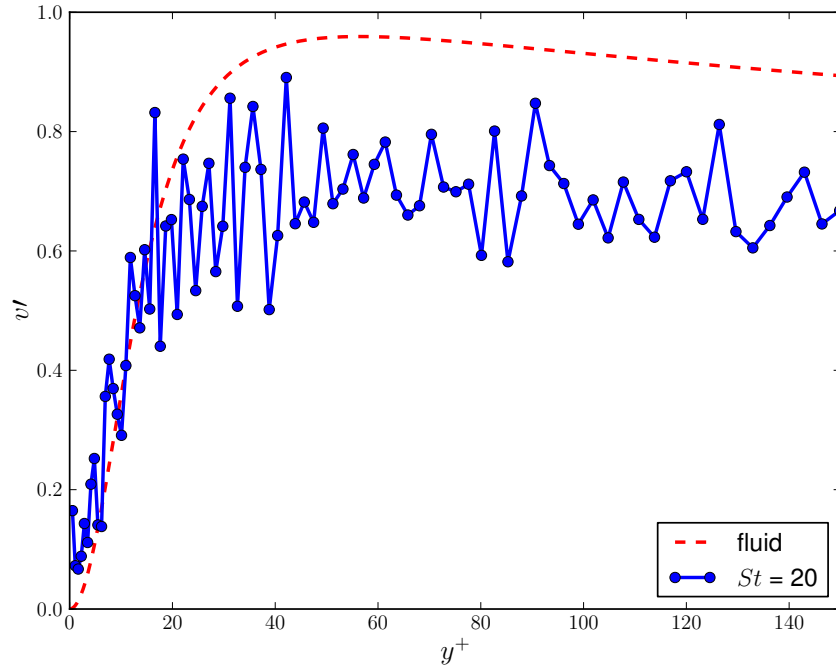


(b)

FIG. 15: Root mean square (r.m.s) of velocity fluctuations, (a) $St = 2$, (b) $St = 5$.



(a)



(b)

FIG. 16: Root mean square (r.m.s) of velocity fluctuations, (a) $St = 10$, (b) $St = 20$.

however, the second population still assumes relatively long near-wall residence time but relatively large deposition velocities. For the first population particles, may be identified as diffusion deposition particles. The near-wall residence time for the second population is different from the DNS data calculated by Narayanan *et al.*¹⁸ as they do not follow the free flight curve defined in Eq: 22. But the magnitude of deposition velocity of this population particles falls into the correct range of $[10^0, 10^{-3}]$ as shown by Narayanan *et al.*¹⁸. For all the deposited particles, the majority falls into the second population. As far as the over-prediction of near-wall residence time compared to the DNS data is concerned, these particles may experience significant repeated events both in quadrant IV (sweeps) and in quadrant II (ejections) within the viscous sublayer, and the events in quadrant II causes particles to be re-entrained to out-layer or to coast along the wall surface within the region of $y^+ < 3$ with relatively larger velocity values before getting deposited. As a consequence, they assume relatively larger velocity values and larger near-wall residence time at the same time.

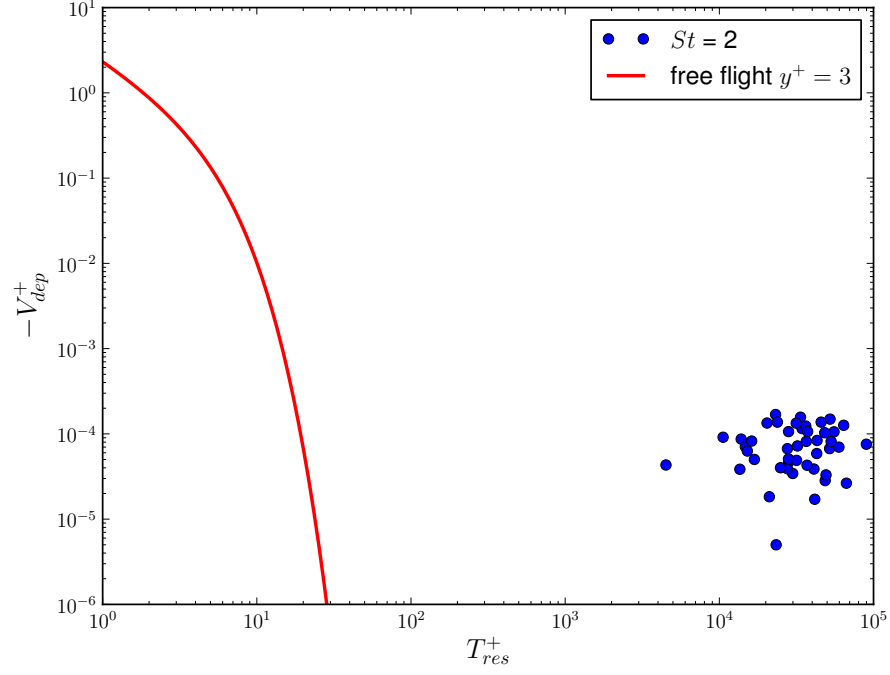
6. A note on the influence of segregation on deposition

This is reflected in the contribution segregation has on the net drift velocity of particles towards the wall and it is the combination of drift versus diffusion away from the wall that leads to a build-up of particle concentration near the wall. The drift velocity is referred to as turbophoresis because when it was first invoked it referred to the migration of particles in an inhomogeneous turbulent flow from regions of high to low regions of turbulence intensity⁵⁶. More precisely the turbophoretic velocity is given by

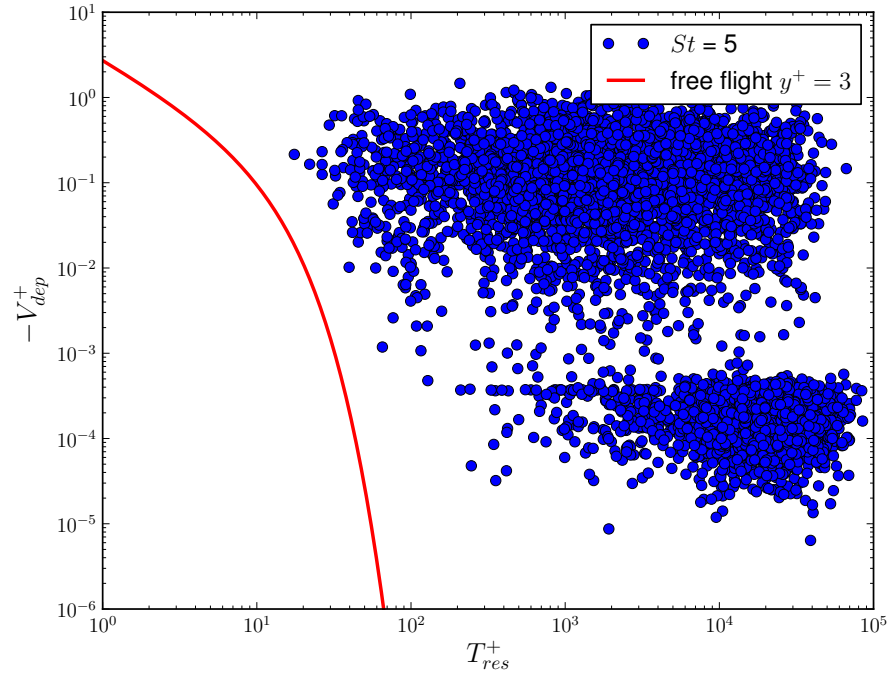
$$v_{t,i} = -\tau_p \frac{\partial \langle v'_j v'_i \rangle}{\partial x_j} \quad (23)$$

where $\langle v'_j v'_i \rangle$ are the particle kinetic stresses per unit mass and τ_p is the particle relaxation or response time. The formula reflects a balance between the drag and the gradients of the particle kinetic stress at equilibrium. In the case of a fully developed boundary layer, the drift velocity towards the wall simply reduces to $v_t = -\tau_p d \langle v'^2 \rangle / dy$. It has nothing to do directly with the persistence or scale of the turbulent structures in the flow that is the direct cause of segregation..

The influence of segregation (un-mixing) has been shown to manifest itself as an extra



(a)



(b)

FIG. 17: Particle residence time in the region of $y^+ < 3$ versus particle deposition velocity

(a) $St = 2$, (b) $St = 5$.

drift that depends upon the compressibility of the particle velocity flow field along a particle trajectory⁵⁸: Reeks has referred to it as Maxey drift because it is the same expression for the enhancement of settling under gravity due to turbulent structures in a homogeneous turbulent flow⁵⁹. For a flow field generated by a Langevin equation involving a white noise driving force, the drift is zero because the flow field generated has no structure to it (it has zero spatial correlation). The turbulent flow field generated in this simulation does give rise to an extra drift other than that due to turbophoresis⁵⁶ because it has persistence both in space and time and is spatially inhomogeneous. However it is likely that in real boundary layer flows the combination of vorticity and straining would lead to more pronounced segregation, a greater enhanced drift and to greater deposition rates than predicted by current stochastic CRW models.

7. Probability density function (pdf) of impact velocities of particles

FIGs. 18 and 19 show the PDF of non-dimensional wall-normal impact velocities of depositing particles onto the wall. It is observed that there is a large increase in probability in the first bin for the three sets of particles. The particles falling in this bin may be associated with the population of depositing particles by diffusion. There also exists long trail of high impact velocities, indicating some of the depositing particles have high deposition velocities. They may be associated with free-flight particles. The PDF of $St = 20$ is much wider than those of $St = 5, 10$, indicating that heavier particles are transported by free-flight across the viscous sublayer before deposition⁶⁰.

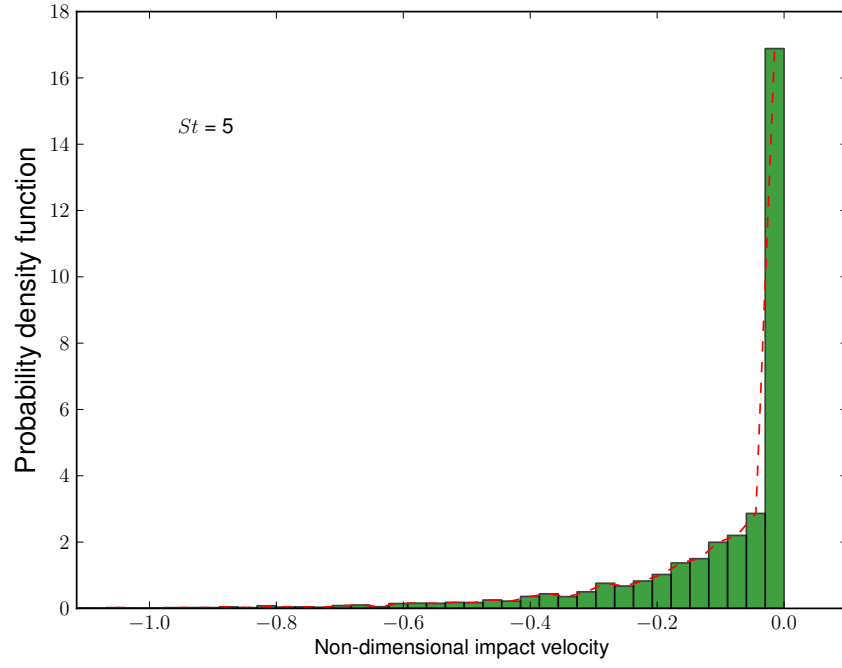
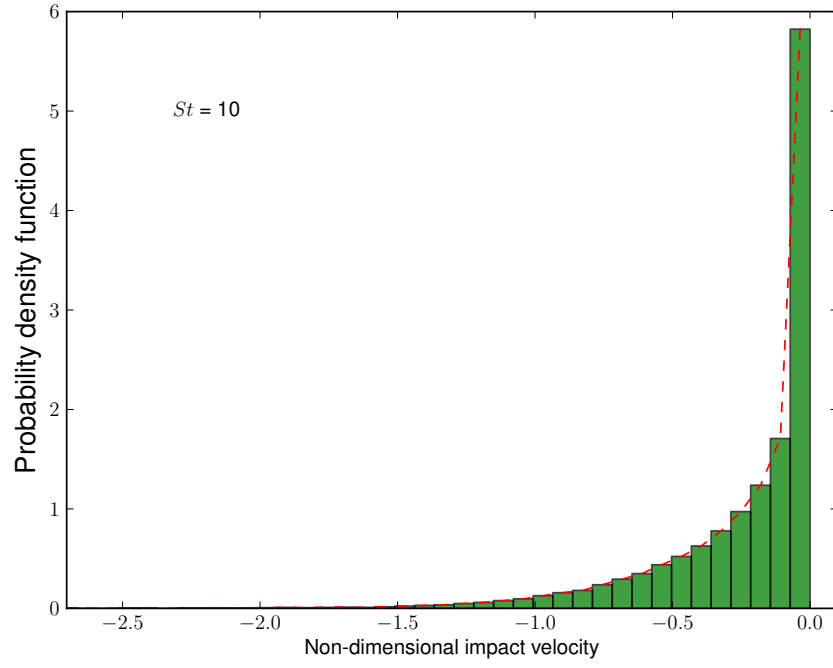
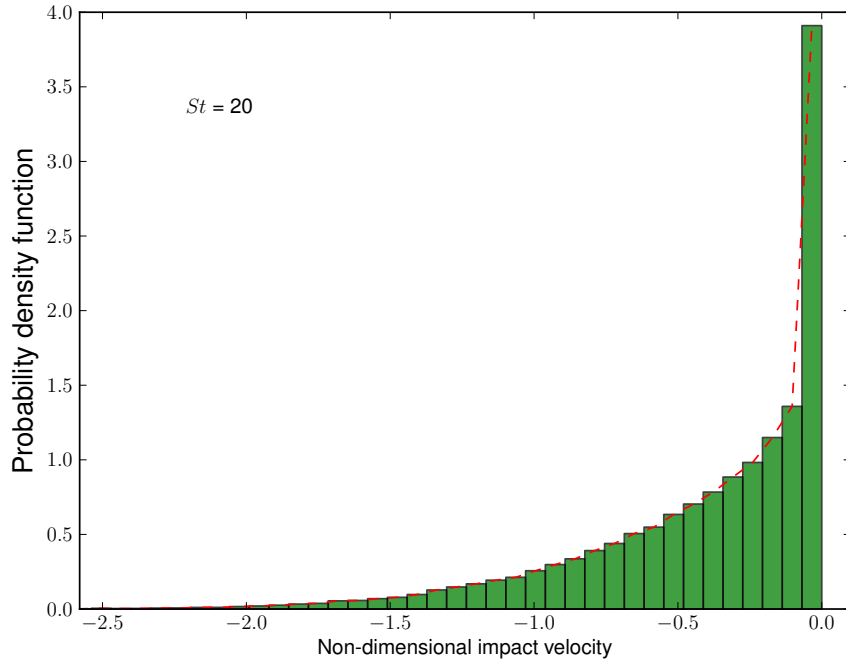


FIG. 18: Probability density function (pdf) of non-dimensional impact velocities of particles, $St = 5$.



(a)



(b)

FIG. 19: Probability density function (pdf) of non-dimensional impact velocities of particles, (a) $St = 10$, (b) $St = 20$.

IV. CONCLUDING REMARKS

We have described a novel stochastic quadrant model for investigating the transport and deposition of heavy particles in a fully developed turbulent boundary layer. The quadrant model was inspired by the quadrant analysis of Willmarth and Lu¹ associated with the Reynolds shear stress domain. The detailed statistics of each quadrant are based on a quadrant analysis of the wall-normal fluid velocity fluctuations obtained by an LES of a fully developed channel flow. The turbulent dispersion of heavy particles in a fully developed turbulent boundary layer is modeled as interactions of heavy particles with a succession of random eddies generated in four quadrants via a homogeneous Markov chain process and was naturally consistent with the skewness of wall-normal fluid velocity fluctuations observed in fully turbulent developed boundary layers. In so doing the model captures the influence of sweeps and ejections in the near wall region of the boundary layer on the particle deposition process. The model was fully coupled with the steady Navier-Stokes solver in ANSYS FLUENT via a stand-alone Lagrangian stochastic particle tracking module. This model yields very good predictions of the deposition rate for particles $St > 5$ when compared with benchmark experimental measurements. Prediction of deposition rates at lower values of St gives a significant under-estimation and may need further improvement or the addition of Brownian motion. In addition, the deposition rates obtained by the stochastic quadrant model was compared with that acquired by solving a one-dimensional Langevin equation based on a continuous random walk (CRW) model as well as results from other CRW models. The discrepancy between deposition rates for particles $St > 5$ is minor. Of particular significance is the comparison of the present model with a stochastic model based on the Langevin equation accounting explicitly for the strong sweeps and ejections in boundary layer turbulence. The deposition rates for the wide range of particle inertia predicted by the present model fall well within the realm of the same experimental data used by Guingo and Minier²⁹. The present data is statistically consistent with experimental analysis of coherent structures in a turbulent boundary layer and is simple to implement in CFD codes.

Most of the predicted statistics of heavy particles are consistent with experiments or DNS calculations. Preferential particle concentration is observed in the near wall region. This indicates that the present stochastic model is capable of predicting turbophoresis responsible for the build-up of particles. The related mean wallward drift velocity is predicted in

the viscous sublayer. Predicted r.m.s. profiles of heavy particles wall-normal velocity are typically lower than the counterpart of fluid particles. Mechanisms for particle deposition is explored by observing particle residence time versus deposition velocity. The population of depositing particles by diffusion is well reproduced. This is also corroborated by a large increase in probability of deposition velocities in the first bin near zero.

The major drawbacks in the present stochastic models lie in the Lagrangian integral time scales for the random eddies occurred in four quadrants and in the inherent spurious drift associated with discrete random walk models. The latter disadvantages may be corrected by introducing an appropriately component into the particle equation of motion to for the wall-normal fluid velocity fluctuation (see⁶¹). However, the time scales for the events in four quadrants still call for further investigations.

ACKNOWLEDGMENTS

The financial support and advice of British Energy (part of EDF Energy, Barnwood, Gloucester, U.K.) is gratefully acknowledged. However the views expressed in this paper are those of the authors and do not necessarily represent the views of the sponsors. The authors would also like to thank Dr. David C. Swailes for the insightful discussions on the development of the stochastic quadrant model.

REFERENCES

- ¹W. W. Willmarth and S. S. Lu, “Structure of the reynolds stress near the wall,” *Journal of Fluid Mechanics*, **55**, 65–92 (1972).
- ²S. K. Friedlander, *Smoke, Dust, and Haze: Fundamentals of Aerosol Dynamics*, 59New York: *Oxford University Press* (2000).
- ³S. K. Friedlander and H. F. Johnstone, “Deposition of suspended particles from turbulent gas streams,” *Industrial & Engineering Chemistry*, **49**, 1151–1156 (1957).
- ⁴C. N. Davies, “Deposition of aerosols from turbulent flow through pipes,” *Proceedings of the Royal Society of London. Series A, Mathematical and Physical Sciences* (1934-1990), **289**, 235–246 (1966).
- ⁵P. Hutchinson, G. F. Hewitt, and A. E. Dukler, “Deposition of liquid or solid dispersions from turbulent gas streams: a stochastic model,” *Chemical Engineering Science*, **26**, 419–439 (1971).
- ⁶G. A. Kallio and M. W. Reeks, “A numerical simulation of particle deposition in turbulent boundary layers,” *International Journal of Multiphase Flow*, **15**, 433–446 (1989).
- ⁷D. C. Swailes and M. W. Reeks, “Particle deposition from a turbulent flow. i. a steady-state model for high inertia particles,” *Physics of Fluids*, **6**, 3392 (1994).
- ⁸M. W. Reeks, “On a kinetic equation for the transport of particles in turbulent flows,” *Physics of Fluids A: Fluid Dynamics*, **3**, 446 (1991).
- ⁹J. Young and A. Leeming, “A theory of particle deposition in turbulent pipe flow,” *Journal of Fluid Mechanics*, **340**, 129–159 (1997).
- ¹⁰A. Guha, “A unified eulerian theory of turbulent deposition to smooth and rough surfaces,” *Journal of Aerosol Science*, **28**, 1517–1537 (1997).
- ¹¹L. I. Zaichik, N. I. Drobyshevsky, A. S. Filippov, R. V. Mukin, and V. F. Strizhov, “A diffusion-inertia model for predicting dispersion and deposition of low-inertia particles in turbulent flows,” *International Journal of Heat and Mass Transfer*, **53**, 154–162 (2010).
- ¹²P. Nerisson, O. Simonin, L. Ricciardi, A. Douce, and J. Fazileabasse, “Improved cfd transport and boundary conditions models for low-inertia particles,” *Computers & Fluids*, **40**, 79–91 (2011).
- ¹³J. B. McLaughlin, “Aerosol particle deposition in numerically simulated channel flow,” *Physics of Fluids A: Fluid Dynamics*, **1**, 1211 (1989).

- ¹⁴J. W. Brooke, K. Kontomaris, T. J. Hanratty, and J. B. McLaughlin, “Turbulent deposition and trapping of aerosols at a wall,” *Physics of Fluids A: Fluid Dynamics*, **4**, 825 (1992).
- ¹⁵Q. Wang and K. D. Squires, “Large eddy simulation of particle deposition in a vertical turbulent channel flow,” *International Journal of Multiphase Flow*, **22**, 667–682 (1996).
- ¹⁶W. S. J. Uijttewaai and R. V. A. Oliemans, “Particle dispersion and deposition in direct numerical and large eddy simulations of vertical pipe flows,” *Physics of Fluids*, **8**, 2590 (1996).
- ¹⁷H. Zhang and G. Ahmadi, “Aerosol particle transport and deposition in vertical and horizontal turbulent duct flows,” *Journal of Fluid Mechanics*, **406**, 55–88 (2000).
- ¹⁸C. Narayanan, D. Lakehal, L. Botto, and A. Soldati, “Mechanisms of particle deposition in a fully developed turbulent open channel flow,” *Physics of Fluids*, **15**, 763–775 (2003).
- ¹⁹C. Marchioli, A. Giusti, M. Vittoria Salvetti, and A. Soldati, “Direct numerical simulation of particle wall transfer and deposition in upward turbulent pipe flow,” *International Journal of Multiphase Flow*, **29**, 1017–1038 (2003).
- ²⁰C. Greenfield, *Numerical modelling of transport phenomena in reactors*, Ph.D. thesis, Bristol Univesity (1998).
- ²¹E. A. Matida, K. Nishino, and K. Torii, “Statistical simulation of particle deposition on the wall from turbulent dispersed pipe flow,” *International Journal of Heat and Fluid Flow*, **21**, 389–402 (2000).
- ²²C. Kroer and Y. Drossinos, “A random-walk simulation of thermophoretic particle deposition in a turbulent boundary layer,” *International Journal of Multiphase Flow*, **26**, 1325–1350 (2000).
- ²³B. Y. H. Liu and J. K. Agarwal, “Experimental observation of aerosol deposition in turbulent flow,” *Journal of Aerosol Science*, **5**, 145–148, IN1–IN2, 149–155 (1974).
- ²⁴A. Dehbi, “A CFD model for particle dispersion in turbulent boundary layer flows,” *Nuclear Engineering and Design*, **238**, 707–715 (2008).
- ²⁵M. Horn and H. J. Schmid, “A comprehensive approach in modeling lagrangian particle deposition in turbulent boundary layers,” *Powder Technology*, **186**, 189–198 (2008).
- ²⁶L. Tian and G. Ahmadi, “Particle deposition in turbulent duct flows - comparisons of different model predictions,” *Journal of Aerosol Science*, **38**, 377–397 (2007).
- ²⁷S. Parker, T. Foat, and S. Preston, “Towards quantitative prediction of aerosol deposition

- from turbulent flows,” *Journal of Aerosol Science*, **39**, 99–112 (2008).
- ²⁸A. Dehbi, “Turbulent particle dispersion in arbitrary wall-bounded geometries: A coupled CFD-Langevin-equation based approach,” *International Journal of Multiphase Flow*, **34**, 819–828 (2008).
- ²⁹M. Guingo and J. P. Minier, “A stochastic model of coherent structures for particle deposition in turbulent flows,” *Physics of Fluids*, **20** (2008).
- ³⁰S. Chibbaro and J. P. Minier, “Langevin PDF simulation of particle deposition in a turbulent pipe flow,” *Journal of Aerosol Science*, **39**, 555–571 (2008).
- ³¹S. J. Kline, W. C. Reynolds, F. A. Schraub, and P. W. Runstadler, “The structure of turbulent boundary layers,” *Journal of Fluid Mechanics*, **30**, 741–773 (1967).
- ³²P. R. Owen, “Pneumatic transport,” *Journal of Fluid Mechanics*, **39**, 407–432 (1969).
- ³³J. W. Cleaver and B. Yates, “A sub layer model for the deposition of particles from a turbulent flow,” *Chemical Engineering Science*, **30**, 983–992 (1975).
- ³⁴M. Fichman, C. Gutfinger, and D. Pnueli, “A model for turbulent deposition of aerosols,” *Journal of Aerosol Science*, **19**, 123–136 (1988).
- ³⁵F. G. Fan and G. Ahmadi, “A sublayer model for turbulent deposition of particles in vertical ducts with smooth and rough surfaces,” *Journal of Aerosol Science*, **24**, 45–64 (1993).
- ³⁶T. Wei and W. W. Willmarth, “Examination of v-velocity fluctuations in a turbulent channel flow in the context of sediment transport,” *Journal of Fluid Mechanics*, **223**, 241–252 (1991).
- ³⁷D. Kaftori, G. Hetsroni, and S. Banerjee, “Particle behavior in the turbulent boundary layer. i. motion, deposition, and entrainment,” *Physics of Fluids*, **7**, 1095 (1995).
- ³⁸D. Kaftori, G. Hetsroni, and S. Banerjee, “Particle behavior in the turbulent boundary layer. ii. velocity and distribution profiles,” *Physics of Fluids*, **7**, 1107 (1995).
- ³⁹C. Marchioli and A. Soldati, “Mechanisms for particle transfer and segregation in a turbulent boundary layer,” *Journal of Fluid Mechanics*, **468**, 283–315 (2002).
- ⁴⁰A. Soldati and C. Marchioli, “Physics and modelling of turbulent particle deposition and entrainment: Review of a systematic study,” *International Journal of Multiphase Flow*, **35**, 827–839 (2009).
- ⁴¹D. C. Wilcox, *Turbulence Modeling for CFD* (DCW Industries Inc., La Cañada, CA, 1993).
- ⁴²A. Mehel, A. Tanière, B. Oesterlé, and J. R. Fontaine, “The influence of an anisotropic

- langevin dispersion model on the prediction of micro-and nanoparticle deposition in wall-bounded turbulent flows,” *Journal of Aerosol Science*, **41**, 729–744 (2010).
- ⁴³S. B. Pope, *Turbulent Flows* (Cambridge University Press, 2000).
- ⁴⁴J. Kim, P. Moin, and R. Moser, “Turbulence statistics in fully developed channel flow at low reynolds number,” *Journal of Fluid Mechanics*, **177**, 133–166 (1987).
- ⁴⁵M. Germano, U. Piomelli, P. Moin, and W. H. Cabot, “A dynamic subgrid-scale eddy viscosity model,” *Physics of Fluids A: Fluid Dynamics*, **3**, 1760 (1991).
- ⁴⁶J. Kim and P. Moin, “Application of a fractional-step method to incompressible navier-stokes equations,” *Journal of computational physics*, **59**, 308–323 (1985).
- ⁴⁷T. S. Luchik and T. W. G. Tiederman, “Timescale and structure of ejections and bursts in turbulent channel flows,” *Journal of Fluid Mechanics*, **174**, 529–552 (1987).
- ⁴⁸M. R. Maxey and J. J. Riley, “Equation of motion for a small rigid sphere in a nonuniform flow,” *Physics of Fluids*, **26**, 883 (1983).
- ⁴⁹C. Marchioli, M. Picciotto, and A. Soldati, “Particle dispersion and wall-dependent turbulent flow scales: implications for local equilibrium models,” *Journal of Turbulence* (2006).
- ⁵⁰S. A. Morsi and A. J. Alexander, “An investigation of particle trajectories in two-phase flow systems,” *Journal of Fluid Mechanics*, **55**, 193–208 (1972).
- ⁵¹D. D. McCoy and T. J. Hanratty, “Rate of deposition of droplets in annular two-phase flow,” *International Journal of Multiphase Flow*, **3**, 319–331 (1977).
- ⁵²Y. Mito and T. J. Hanratty, “Use of a modified langevin equation to describe turbulent dispersion of fluid particles in a channel flow,” *Flow, turbulence and combustion*, **68**, 1–26 (2002).
- ⁵³T. L. Bocksell and E. Loth, “Stochastic modeling of particle diffusion in a turbulent boundary layer,” *International Journal of Multiphase Flow*, **32**, 1234–1253 (2006).
- ⁵⁴G. N. Mil’shtein, “A method of second order accuracy integration of stochastic differential equations,” *Teoriya Veroyatnostei i ee Primeneniya*, **23**, 414–419 (1978).
- ⁵⁵P. G. Papavergos and A. B. Hedley, “Particle deposition behaviour from turbulent flows,” *Chemical Engineering Research and Design*, **62**, 275–95 (1984).
- ⁵⁶M. W. Reeks, “The transport of discrete particles in inhomogeneous turbulence,” *Journal of Aerosol Science*, **14**, 729–739 (1983).
- ⁵⁷J. W. Brooke, T. J. Hanratty, and J. B. McLaughlin, “Free-flight mixing and deposition of aerosols,” *Physics of Fluids*, **6**, 3404 (1994).

- ⁵⁸M. W. Reeks, “On model equations for particle dispersion in inhomogeneous turbulence,” *International Journal of Multiphase Flow*, **31**, 93–114 (2005).
- ⁵⁹M. R. Maxey, “Gravitational settling of aerosol particles in homogeneous turbulence and random flow fields,” *Journal of Fluid Mechanics*, **174**, 441 (1987).
- ⁶⁰P. van Dijk and D. Swailes, “Hermite-dg methods for pdf equations modelling particle transport and deposition in turbulent boundary layers,” *Journal of Computational Physics*, **231**, 4904 – 4920 (2012), ISSN 0021-9991.
- ⁶¹J. M. MacInnes and F. V. Bracco, “Stochastic particle dispersion modeling and the tracer-particle limit,” *Physics of Fluids A: Fluid Dynamics*, **4**, 2809 (1992).